

# Phasing Diploid Genome Assembly Graphs with Single-Cell Strand Sequencing

Mir Henglin<sup>1,2,\*</sup>, Maryam Ghareghani<sup>3,4,\*</sup>, William Harvey<sup>5</sup>, David Porubsky<sup>5</sup>, Sergey Koren<sup>6</sup>, Evan E. Eichler<sup>5,7</sup>, Peter Ebert<sup>8,1,2,†</sup>, Tobias Marschall<sup>1,2,†</sup>

<sup>1</sup> Institute for Medical Biometry and Bioinformatics, Medical Faculty and University Hospital Düsseldorf, Heinrich Heine University Düsseldorf, Germany

<sup>2</sup> Center for Digital Medicine, Heinrich Heine University Düsseldorf, Germany

<sup>3</sup> Department of Mathematics and Computer Science, Freie Universität Berlin, Germany

<sup>4</sup> Department of Computational Molecular Biology, Max Planck Institute for Molecular Genetics, Berlin, Germany

<sup>5</sup> Department of Genome Sciences, University of Washington School of Medicine, Seattle, WA, USA

<sup>6</sup> Genome Informatics Section, Computational and Statistical Genomics Branch, National Human Genome Research Institute, National Institutes of Health, Bethesda, MD, USA

<sup>7</sup> Howard Hughes Medical Institute, University of Washington, Seattle, WA, USA

<sup>8</sup> Core Unit Bioinformatics, Medical Faculty and University Hospital Düsseldorf, Heinrich Heine University Düsseldorf, Germany

\* joint first authorship

† joint last/corresponding authorship, [peter.ebert@hhu.de](mailto:peter.ebert@hhu.de), [tobias.marschall@hhu.de](mailto:tobias.marschall@hhu.de)

## Abstract

Haplotype information is crucial for biomedical and population genetics research. However, current strategies to produce *de-novo* haplotype-resolved assemblies often require either difficult-to-acquire parental data or an intermediate haplotype-collapsed assembly. Here, we present Graphasing, a workflow which synthesizes the global phase signal of Strand-seq with assembly graph topology to produce chromosome-scale *de-novo* haplotypes for diploid genomes. Graphasing readily integrates with any assembly workflow that both outputs an assembly graph and has a haplotype assembly mode. Graphasing performs comparably to trio-phasing in contiguity, phasing accuracy, and assembly quality, outperforms Hi-C in phasing accuracy, and generates human assemblies with over 18 chromosome-spanning haplotypes.

## Keywords

*de-novo* Assembly, Phasing, Assembly Graph, Haplotype, Strand-seq, Hi-C, Trio, Verkko, hifiasm,

## Background

Many eukaryotic organisms are diploid, and carry two sets of pairwise-similar chromosomes, with one set inherited from each parent. Consequently, separately assembling the two copies of each chromosome is necessary to fully characterize an individual's genome. Each version of a chromosome inherited from a parent is called a *haplotype*. The process of assigning the two alleles of a heterozygous variant to their corresponding haplotype is termed *phasing*.

Haplotype-resolved genome assemblies provide crucial insights into studies of disease, evolution, and biodiversity by revealing segregation patterns of alleles within and between haplotypes [1]. Medically important genes and genomic regions, such as the major histocompatibility complex and *APOE* gene, exhibit compound heterozygosity, where alleles carried on the same haplotype produce a phenotype different than when those same alleles are carried on different haplotypes [2,3]. Haplotype-resolved assemblies support research on evolution, gene flow, demography, gene expression, and conservation biology [4–6], where knowledge of haplotype-specific combinations of genomic variants can be of crucial importance.

Despite their utility, it remains a major challenge to produce haplotype-resolved genome assemblies for diploid organisms. The ability of an assembler to phase genomic variation is directly tied to the length of the reads used to construct the assembly. As any single read originates from a single haplotype, any read that spans multiple heterozygous variants forms a “local” haplotype which can, in principle, be stitched into longer haplotype segments through the assembly of overlapping reads [2]. However, in practice this process is affected by both sequencing errors and ambiguities due to repetitive sequence. Correspondingly, advances in long-read genome sequencing technologies have led to improved genome assemblies, as read lengths are now long enough to span a greater range of repetitive DNA variation [7]. Pacific Biosciences (PacBio) High-Fidelity (HiFi) reads [8] are 15–20 kb in length and have an error rate similar to accurate short-read sequencing, and Oxford Nanopore Technologies (ONT) Ultra-long reads [9] can achieve lengths > 100 kbp, which is long enough to span the majority of repeats found in human DNA. However, these read lengths are still too short to produce fully haplotype-resolved assemblies, even for assemblers utilizing combinations of long-read sequencing technologies [10,11]. Further computational steps and data sources beyond those employed in a “standard” genome assembly workflow are required in order to construct fully phased haplotypes [1,12–14].

When phasing with short, noisy, or low-coverage reads, reference-mapping-based methods are commonly used. Many phasing tools, such as WhatsHap [15], HapCol [16], HapCut2[17], MarginPhase [18], and LongPhase [19] utilize this strategy, where reads are first aligned to a reference genome and genomic variants are called. Subsequently, the variants are used to separate reads by haplotype for haplotype-specific assembly. The reference mapping approach is necessarily subjected to reference bias, and can therefore fail when variant calling is challenging due to unreliable alignment of reads to

the reference, which occurs due to repetitive sequence or when the reference and sample differ in large structural variation [20]. Reference bias can be avoided by first constructing an unphased *de-novo* assembly to serve as the reference genome for genomic variant calling and phasing. This *de-novo* reference strategy is employed by the phasebook assembler [21], PGAS[22] and DipASM[22,23], where the latter two additionally leverage the long-range haplotype signal from Strand-seq [24,25] and Hi-C [26] data respectively to improve the haplotypes constructed with this strategy. However, the *de-novo* reference, being yet unphased, is a mosaic reference produced by collapsing sequence from both haplotypes together, which can introduce switch errors, false duplications, and nucleotide consensus errors [1,27–30].

When parental data is available, trio-binning can be used to assemble haplotypes without use of a reference genome. Trio-binning approaches use parental reads to identify “hap-mers”, k-mers unique to the maternal and paternal haplotypes, to label and partition reads before assembly [31]. Because trio-binning is reference-free, it avoids the errors introduced through the creation of a collapsed assembly. However, the difficulty and expense of acquiring and sequencing three individuals' genetic information limits trio-binning's widespread application. Furthermore, trio-binning of reads before assembly is vulnerable to false duplications and fragmentation [32] and can be limited in its ability to phase repetitive or homozygous regions, which have few haplotype-specific k-mers [31,33].

Instead of binning reads by haplotype prior to assembly, performing the phasing directly on the assembly graph has emerged as an attractive strategy. Graph-based phasing typically combines the phase signal inherent to an assembly graph with an additional source of phase information [12,32,34], avoiding the errors introduced by the binning of reads before assembly while usually yielding larger phasing blocks. Typically, long-range phasing information from trio, Hi-C, or Strand-seq is aligned to the graph and synthesized with the graph topology to construct haplotypes. Trio and Strand-seq methods have the advantage of global phase signal, in contrast to the local phase signal of Hi-C, the strength of which diminishes with distance. Recent long read assemblers such as hifiasm [10], Verkko [11], and Shasta [33], all natively support trio and Hi-C data integration, and trio-based assemblies from hifiasm and Verkko are currently the highest-quality phased assemblies that can be produced. Recently, independent modules which employ trio or Hi-C graph-based phasing have emerged, such as GreenHill [35] and GFAs [33]. These modules are designed to integrate with a wide range of assemblers, and can provide graph-based phasing capabilities to diverse workflows.

## Contribution

We present Graphasing, a Strand-seq alignment-to-graph-based phasing and scaffolding workflow that assembles telomere-to-telomere (T2T) human haplotypes using data from a single sample. Graphasing leverages a robust cosine similarity clustering approach to synthesize global phase signal from Strand-seq alignments with assembly graph topology, producing accurate haplotype calls and end-to-end scaffolds. We built assemblies for the NA24385 (HG002) and HG00733 genomes using Graphasing with the Verkko and hifiasm assemblers and compared the quality of the haplotypes with

those constructed by native trio and Hi-C mode, and show that our method produced the highest-quality single-sample assemblies, which match or exceed trio-phasing in contiguity, phasing accuracy, and assembly quality.

Graphasing is implemented using the open source workflow language, Snakemake [36]. The pipeline takes as input an assembly graph in .gfa format and a set of Strand-seq libraries in .fasta format, and outputs a haplotype partition of the assembly graph, which can readily be used by assembly tools to produce a final assembly, as well as Strand-seq annotations that can facilitate further downstream analysis. Graphasing is available at <https://github.com/marschall-lab/strand-seq-graph-phasing>

## Results

### Graph-phasing method

Graphasing phases an assembly graph produced by an assembly tool such as Verkko or hifiasm. The Graphasing workflow can be summarized in five main steps:

1. Alignment of Strand-seq reads to assembly unitigs (Figure 1a),
2. Clustering of unitigs by chromosome (Figure 1b),
3. Correction of misoriented unitigs (Figure 1c),
4. Pooling of haplotype informative reads to shade the assembly graph (Figure 1d),
5. Threading of haplotypes through the shaded graph to phase and scaffold the assembly (Figure 1d).

Strand-seq is a short-read, single-cell sequencing method that generates sequencing libraries derived from only one DNA strand from each chromosome [24]. Consequently, alignments of those reads back to the genome convey a global haplotype signal through the direction of the alignments [22,37–42] (Figure S1). However, though all reads can be used for clustering and misorientation correction, only reads aligning to unique sequence in the assembly carry phase signal, and these phase-informative reads are identified after alignment (Figure 1a). Unitig clustering by chromosome takes a two-step approach. First, a discrete clustering algorithm is applied to the unitigs with the clearest phasing signal (Figure 1b). This initial clustering then anchors an agglomerative cosine-similarity clustering strategy that clusters the remaining unitigs. Next, a hierarchical cosine-similarity clustering strategy is applied to identify misoriented unitigs in each chromosome cluster (Figure 1c). Finally, the phase-informative reads are used in a self-supervised classification model to produce a haplotype shading of the assembly graph based on the pooled Strand-seq libraries (Figure 1d). Rukki [11] then threads the shaded graph to produce haplotype calls and scaffolds, which can bridge tangles and gaps in the assembly. Verkko directly accepts the output scaffolds as input to produce a phased assembly, while for hifiasm, phasing information is communicated by using the haplotype calls to construct k-mer databases that are passed to trio-mode assembly. Details of each step are described in the [Methods](#) section.

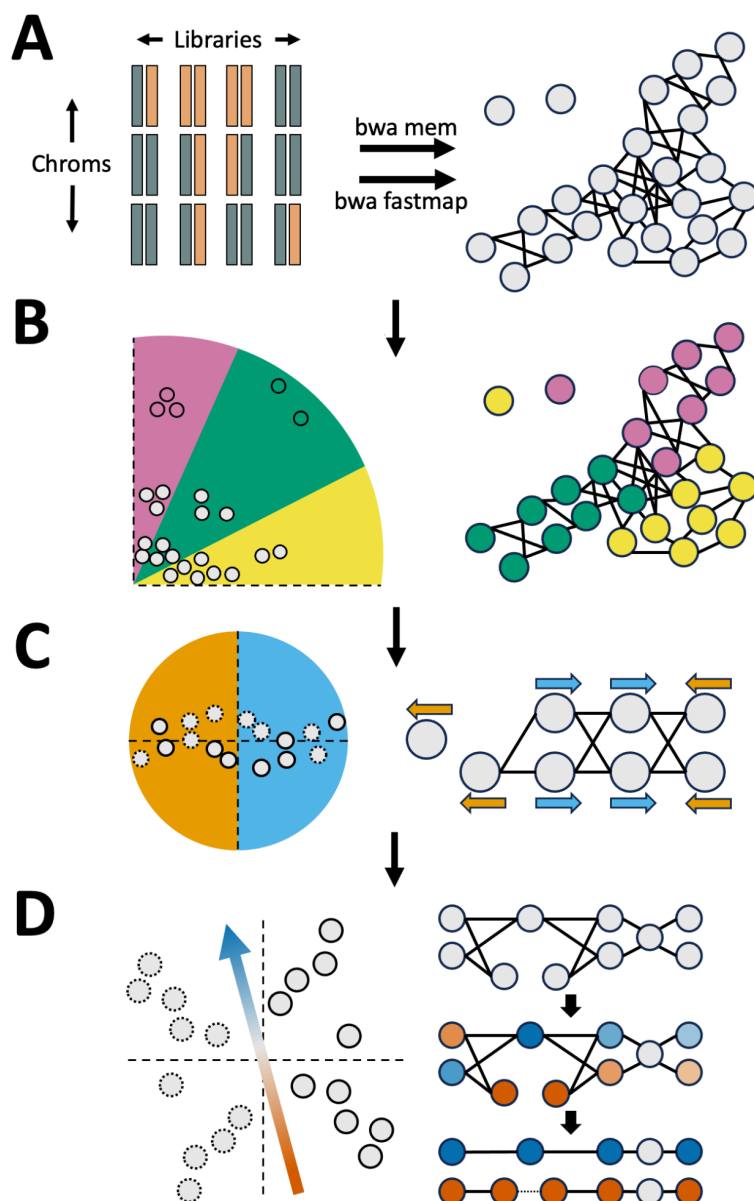


**Figure 1. Pipeline overview.** **A.** Reads from Strand-seq libraries are aligned to graph unitigs (gray circles) using `'bwa mem'` and `'bwa fastmap'`. `'bwa fastmap'` alignments are used to identify haplotype informative reads, which are used for step "D". **B.** Unitigs with strong signal (colored points) are identified and anchor the cosine-similarity chromosome clustering of unitigs with weaker signal (gray points). **C.** Unitigs (solid outline) and their flipped inverses (dotted outline) are used to correct misoriented unitigs. Unitigs in opposite orientation form a bisected structure that is captured with cosine-similarity clustering. **D.** A model is trained to classify unitigs (solid outline) and their flipped versions (dotted outline). The vector describing the decision boundary is used to pool Strand-seq libraries and produce a haplotype shading of the assembly (right, middle). Rukki is run on the shaded graph to produce haplotype calls and scaffolds (right, bottom). Tangles and gaps are bridged, as indicated by the dotted line in the red haplotype.

## Phasing Method Comparison

We compared the performance of Strand-seq based Graphasing to the results of the native trio and Hi-C phasing modes of Verkko and hifiasm. Assemblies were constructed for the NA24385 and HG00733 samples using the Verkko (v. 1.4.1) and hifiasm (v. 0.19.6) phasing pipelines. Hybrid assembly graphs were constructed with 118.1x coverage PacBio HiFi CCS reads [8] and 34.3x (6.3x >100kbp) coverage Oxford Nanopore Technologies (ONT) reads [9] for NA24385, and with 68.3x coverage PacBio HiFi CCS reads and 51.0x (32.8x >100kb) coverage Oxford nanopore for HG00733. Trio phased assemblies were constructed with parental short-read Illumina data at 30x coverage. Strand-seq phased assemblies were constructed by inputting the unphased assembly graphs to Graphasing, using 192 libraries for NA24385 and 115 libraries for HG00733.

## Contiguity

Assembly contiguity was evaluated using N50 and auN. N50 is the most commonly reported metric of contiguity, and is defined as the length of the shortest contig for which longer and equal-length contigs cover more than 50% of the assembly [43], while the auN is a weighted sum of all Nx values for x between 0 and 100 [44]. It is important to note that Strand-seq and Hi-C phasing produce Haplotypes with Parentage Unknown (HaPUs), meaning that while each contig is haplotype-resolved, the parent-of-origin is unknown, unless further methods are employed [45]. For the purposes of comparison, each HaPU was therefore assigned a maternal or paternal label corresponding to the majority of hap-mers occurring on the haplotype. Furthermore, the hifiasm assemblies were not scaffolded, while Verkko produces scaffolds, and so the Verkko assemblies were evaluated both on the scaffolds, and on the resulting scaftigs after breaking scaffolds at gaps.

We found that all phasing methods produced highly contiguous haplotypes, with hifiasm auN ranging from 89.5 Mbp to 131.7 Mbp, Verkko auN ranging from 45.2 Mbp to 135.9 Mbp and Verkko scaffold auN ranging from 122.8 Mbp to 148.7 Mbp (Table 1). To evaluate that improvement gained through each phasing method, we constructed haplotypes from the unphased assemblies by assigning contigs to “maternal” or “paternal” haplotypes according to the majority of hap-mers occurring on each contig. Each haplotype was substantially more contiguous than their unphased counterpart, having an N50 and auN at least 3-times larger, with larger gains observed for NA24385, which had a less contiguous input. Verkko scaffolds had an auN 1 Mbp to 90 Mbp larger than their corresponding contig values, with a mean increase of 38 Mbp. Notably, the NA24385 scaffolds were more contiguous than the HG00733 scaffolds despite a less contiguous input graph, which investigations attributed to the presence of “hairpin-capped broken bubbles” in the center of the largest HG00733 chromosomes which fragmented some of the Rukki scaffolds (Figure S2).

Sample	Assembler	Phasing	Mat N50 (Mbp)	Pat N50 (Mbp)	Mat auN (Mbp)	Pat auN (Mbp)
HG00733	hifiasm Hybrid	Trio	100.7	104.2	99.7	111.5

HG00733	hifiasm Hybrid	Strand-seq	103.4	111.1	102.3	114.8
HG00733	hifiasm Hybrid	Hi-C	136.6	133.3	130.1	131.7
HG00733	hifiasm Hybrid	Unphased	6.8	6.9	7.9	8.2
HG00733	Verkko Hybrid	Trio	104.4 (133.6)	102.4 (104.4)	109.9 (122.8)	116.6 (125.2)
HG00733	Verkko Hybrid	Strand-seq	134.9 (135.3)	110.4 (146.0)	126.4 (130.5)	135.9 (148.7)
HG00733	Verkko Hybrid	Hi-C	134.9 (143.5)	136.7 (136.7)	131.6 (144.7)	134.3 (135.2)
HG00733	Verkko Hybrid	Unphased	27.5	26.1	28.5	28.1
NA24385	hifiasm Hybrid	Trio	95.8	92.4	102.3	95.7
NA24385	hifiasm Hybrid	Strand-seq	89.4	99.2	89.5	103.2
NA24385	hifiasm Hybrid	Hi-C	108.5	103.0	112.8	100.5
NA24385	hifiasm Hybrid	Unphased	1.9	1.9	4.5	2.6
NA24385	Verkko Hybrid	Trio	38.6 (143.8)	36.8 (135.6)	50.6 (138.4)	45.2 (135.6)
NA24385	Verkko Hybrid	Strand-seq	81.5 (144.0)	90.0 (137.8)	76.4 (145.5)	94 (146.0)
NA24385	Verkko Hybrid	Hi-C	80.2 (143.9)	87.2 (135.4)	87.1 (144.1)	89.1 (140.4)
NA24385	Verkko Hybrid	Unphased	3.5	3.4	8.0	4.0

*Table 1. Assembly Contiguity Statistics. Phased Verkko assemblies list two numbers: the contig statistic first, and the scaffold statistic in parentheses second.*

## Nx Curves

For additional insight, we plotted each haplotype's Nx curve [46], which is created by plotting all Nx values, and additionally compared them against two high-quality reference assemblies: NA24385 was compared against the Q100 Project v1.0 NA24385 assembly [47,48] and HG00733 was compared against the T2T v2.0 CHM13 assembly [49].

Inspecting the Nx curves (Figure 2), we see that the Verkko NA24385 Nx curves are mostly equidistant from the reference along the entire length of the curve, roughly indicating equivalent phasing performance at all lengths in the assembly. In contrast, the HG00733 and hifiasm NA24385 assemblies are much closer to the reference curve on the left side of the plots than on the right, indicating a relative dip in contiguity after the very largest contigs. Nonetheless, it is apparent from our results that for each sample and assembler, each phasing method outputs haplotypes with comparable continuity. The Verkko NA24385 scaffold curves in particular diverge from one another less than other sets of curves. The largest differences between Nx curves occurs on the very left of the plots, indicating that the differences in contiguity statistics between haplotypes may mostly stem from differential phasing of the few very largest sequences in the assembly graph. The one exception is the Verkko NA24385 trio contigs, which are noticeably less contiguous than the Hi-C and Strand-seq assemblies

despite similar scaffold contiguity. Of additional note are the Verkko NA24385 scaffolds, which track very closely to the highly polished Q100 standard along the entire Nx curve, and the hifiasm HG00733 Hi-C assembly, which assembled chromosome-scale contigs for chromosomes 1 and 2 for both haplotypes. One unusual feature is that the NA24385 hifiasm and Verkko Hi-C Nx curves exceed the reference on the left side of the plot. This occurred because Strand-seq and Hi-C produces HaPUs, and consequently a contig may be compared to the reference of different parental origin.

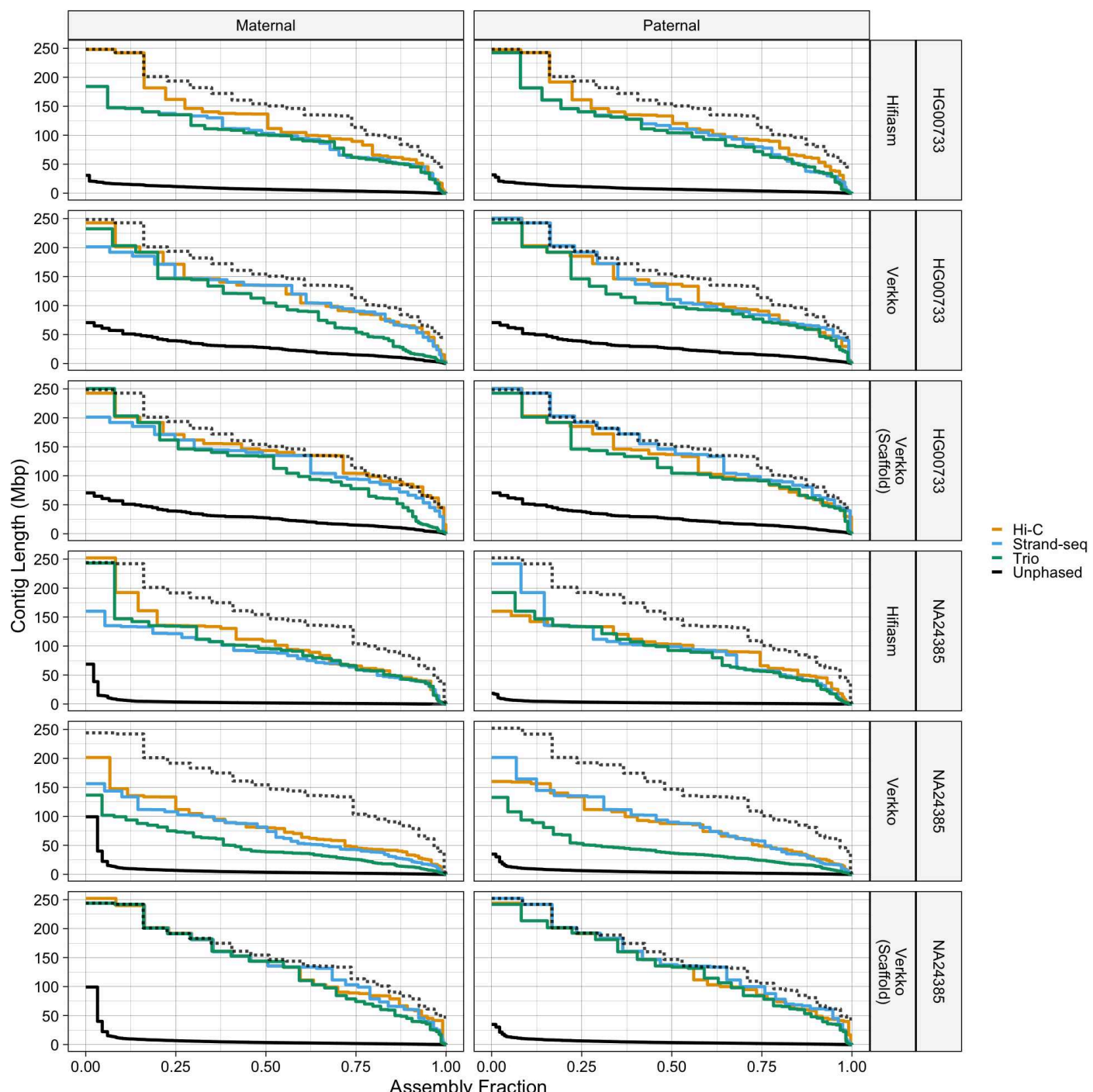


Figure 2. Nx curves. Columns from left to right correspond to maternal and paternal haplotypes, and rows from top to bottom correspond to HG00733 and NA24385 for each assembler. The dotted black lines correspond to the reference standards, which are the Q100 v1.0 assembly for NA24385, and the CHM13 v2.0 assembly for

HG00733. Because there is only one CHM13 haplotype, the dotted reference line is the same in the maternal and paternal HG00733 facets. The solid black lines correspond to the unphased assemblies.

## End-to-End Haplotypes

We further investigated each assembly for the number of end-to-end haplotypes. After using minimap2 [50,51] to align the assemblies to their respective references, the CHM13 v2.0 assembly for HG00733 and the Q100 v1.0 assembly for NA24385, three different properties were evaluated. If the summed alignment length was within 5% of the length of both the contig or scaffold and the reference chromosome, it was labeled “chromosome-scale”. If ‘seqtk telo’ [52] detected telomeric repeats at both ends of a contig or scaffold, it was labeled as having two telomeres. Finally, if a contig or scaffold mapped to the reference in one contiguous alignment, it was labeled “unbroken”. Unbroken alignments were only expected for the NA24385 assemblies, as they were aligned to a reference of the same genome. A contig or scaffold satisfying both of the first two properties was considered “chromosome-spanning”, while a contig or scaffold satisfying all three properties was considered to be “telomere-to-telomere” (T2T).

We found that for HG00733, the Verkko assemblies produced more chromosome-spanning contigs than did the hifiasm assemblies, and vice-versa for NA24385, stemming from the more contiguous input for HG00733 (Table 2). hifiasm assemblies each contained 8-16 chromosome-spanning contigs while the Verkko assemblies each contained 0-17 chromosome-spanning contigs. All Verkko NA24385 end-to-end contigs were also T2T, while most hifiasm NA24385 end-to-end contigs aligned to the reference in multiple pieces. Scaffolding greatly increased the number of chromosome-spanning sequences, and the Verkko assemblies each contained 14-21 chromosome-spanning scaffolds, 4-20 more than the corresponding number of contigs, with an especially large increases of 9, 14, and 20 for NA24385, highlighting the advantages of scaffolding for the less contiguous input assembly.

Sample	Assembler	Phasing	Chromosome-Scale (n)	Chromosome-Scale w/ Two Telomeres (n)	Chromosome-Scale w/ Two Telomeres & Unbroken (n)
HG00733	hifiasm Hybrid	Trio	15	8	NA
HG00733	hifiasm Hybrid	Strand-seq	16	9	NA
HG00733	hifiasm Hybrid	Hi-C	21	16	NA
HG00733	Verkko Hybrid	Trio	14 (21)	11 (15)	NA (NA)
HG00733	Verkko Hybrid	Strand-seq	21 (27)	16 (20)	NA (NA)
HG00733	Verkko Hybrid	Hi-C	21 (26)	17 (21)	NA (NA)
NA24385	hifiasm Hybrid	Trio	13	9	3
NA24385	hifiasm Hybrid	Strand-seq	12	8	2

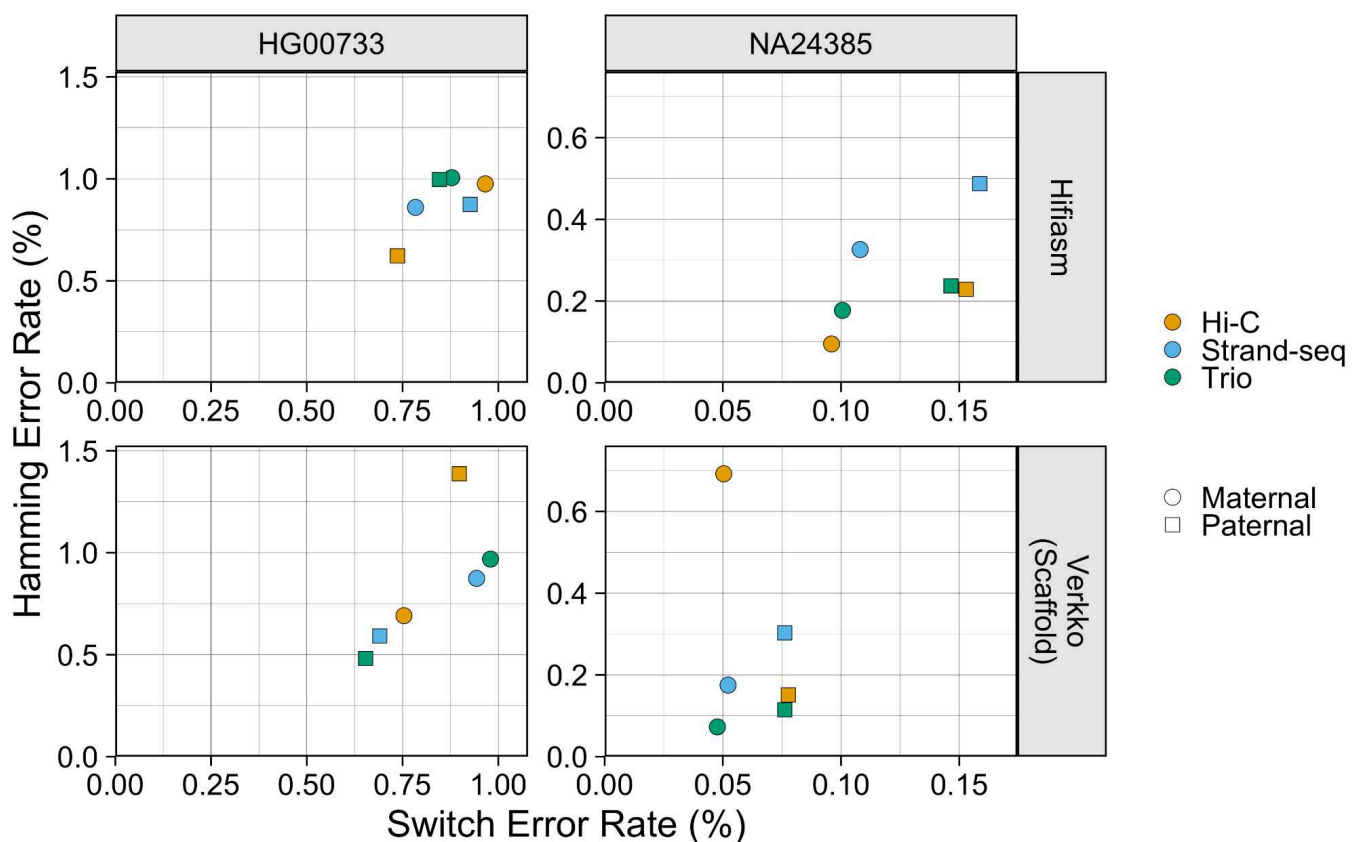
NA24385	hifiasm Hybrid	Hi-C	16	11	7
NA24385	Verkko Hybrid	Trio	0 (27)	0 (20)	0 (1)
NA24385	Verkko Hybrid	Strand-seq	6 (29)	4 (18)	4 (4)
NA24385	Verkko Hybrid	Hi-C	7 (26)	5 (14)	5 (5)

Table 2. End-to-end haplotype counts. Phased Verkko assemblies list two numbers: the contig statistic first, and the scaffold statistic in parentheses second.

## Phasing Accuracy

Yak [32] was used to calculate the switch error rate and Hamming error rate. Yak utilizes parental sequence data to identify hap-mers and create a haplotype coloring of the assembly contigs and estimate switch and Hamming errors. To avoid inflation of the trio assemblies' performance, the data used for error rate calculation was independent of the data used for trio phasing. For HG00733, hap-mers were identified from orthogonal parental Illumina sequencing data, and for NA24385, hap-mers were identified from the Q100 Project v1.0 assembly. The Q100 assembly is the highest quality NA24385 assembly publicly available, with an estimated error rate below 1 per 10 million bases [53]. For the Verkko assemblies, only scaffolds were evaluated in this and all subsequently described evaluations.

The haplotypes produced by hifiasm and Verkko were generally high-quality and had a low error rate (Figure 3). The Verkko Strand-seq and trio assemblies were the best performing assemblies for both HG00733 and NA24385, with switch and Hamming error rates below 1% for HG00733 and switch error rates below 0.08% and Hamming error rates below 0.3% for NA24385. The Verkko Hi-C assemblies, despite having a similar switch error rate as the other Verkko assemblies, each had a haplotype with a high Hamming error; the paternal HG00733 and the maternal NA24385 haplotypes had Hamming error rates about 1.5 and 3 times that of the other phasing methods respectively, resulting from large, balanced switch errors (Figure 4). The hifiasm assembly switch and Hamming error rates for NA24385 ranged from 0.096% to 0.16% and 0.095% to 0.49% respectively, and from 0.74% to 0.93% and 0.62% to 1.01% respectively for HG00733. For NA24385, each Verkko haplotype had a switch error on average 0.06pp lower than the corresponding hifiasm haplotype which, though small in absolute terms, represents an almost 2-fold difference in the switch error rate. For HG00733, the differences were smaller both in absolute and relative magnitude, where on average the Verkko haplotypes had a switch error rate 0.04pp lower than the corresponding hifiasm haplotypes. A notable feature is that the NA24385 error rates are an order of magnitude less than the error rates of the HG00733 haplotypes. We believe that a large portion of the difference between the HG00733 and NA24385 error rates is due to the more accurate evaluation of the NA24385 haplotypes provided through the highly curated Q100 assembly, which suggests that the true error rates for the HG00733 assemblies may be lower than presented here.



*Figure 3. Haplotype Error Rate Scatter* The X-coordinate of each point is the estimated switch error rate for a haplotype, and the y-coordinate is the estimated Hamming error rate. Points are colored by phasing data, and shape corresponds to haplotype.

To further investigate the phasing accuracy of the haplotypes, we produced hap-mer blob plots [54]. In a hap-mer blob plot, properly phased contigs, which contain hap-mers from only one parent, will be found on the X- or Y- axis. Any blob not on either axis contains a mixture of sequence from both parents, and contigs containing an equal mixture of parental hap-mers will be found on the gray line. Inspection of the blob plots revealed only the Verkko Hi-C assemblies had large, balanced switch errors, as the HG00733 and NA24385 assemblies each had single contig 185 and 42 Mbp in size respectively which strongly deviated from the axes (Figure 4). Smaller deviations from the axis can be observed in the other assemblies, but represent much smaller Hamming errors. Unitigs aligning to the X and Y chromosomes in the NA24385 assemblies received many more hap-mer alignments than unitigs aligning to the autosomes. By inspecting the sex unitig blobs, we see that the X and Y chromosomes are represented in one scaffold in the Verkko assemblies (Figure S3).

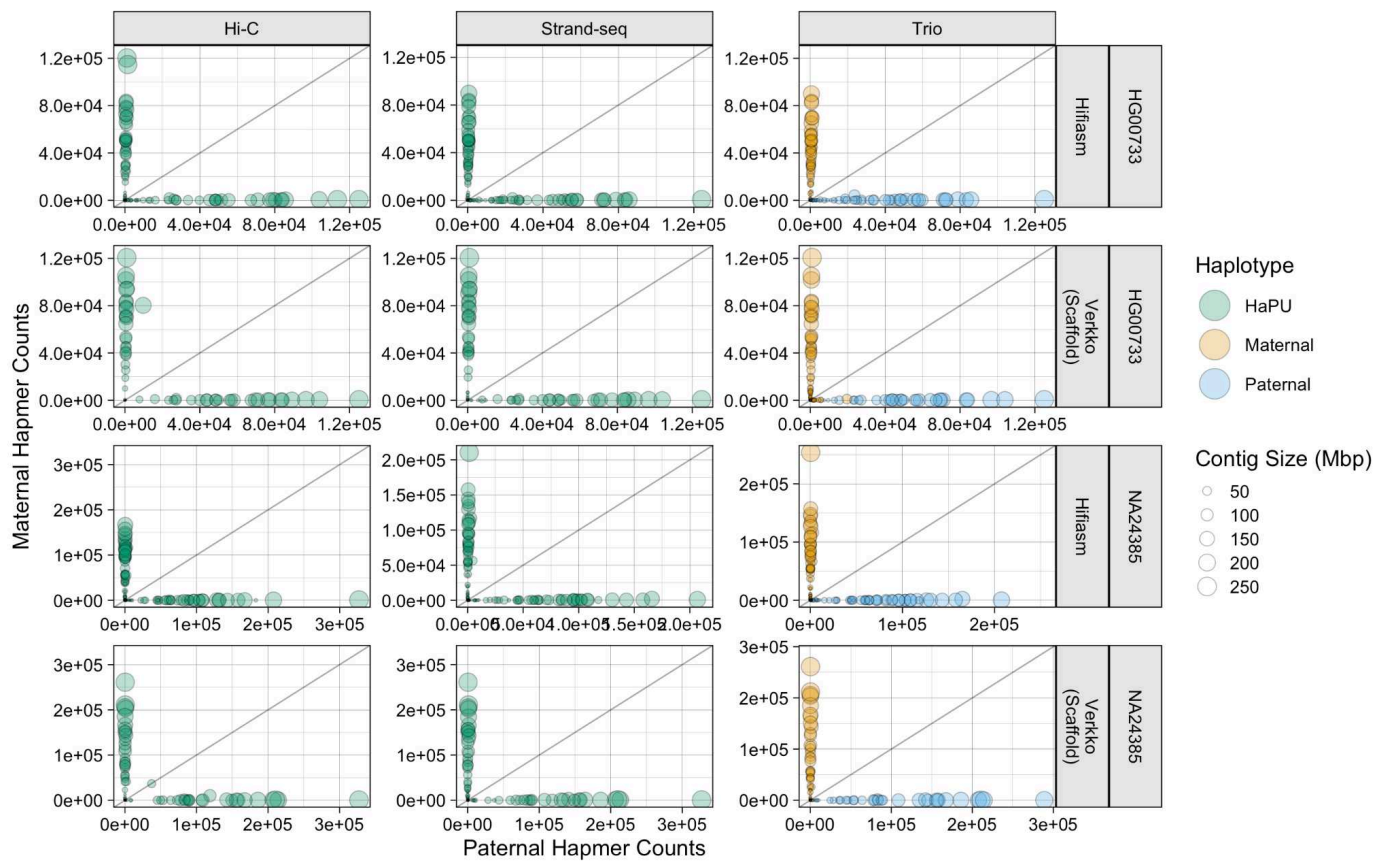


Figure 4. Hap-mer Blob Plots. For the NA24385 assemblies, only contigs aligning to autosomal chromosomes are plotted. The X- and Y-coordinate of each point is the number of hap-mers occurring on the contig, and the size of each point corresponds to contig length. Green points correspond to the Strand-seq and Hi-C HaPUs, while orange points correspond to the trio maternal haplotype, and blue points to the trio paternal haplotype. The grey line is the line of equality, where the number of hap-mers from either parent occurring on a contig is equal. The greater the phasing accuracy, the closer a blob is aligned to each axis.

## Consensus Quality

Consensus sequence quality value (QV) was estimated with Yak using orthogonal Illumina sequencing data for HG00733 and the Q100 v1.0 assembly for NA24385. Yak estimates the QV by comparing assembly k-mers to reference k-mers, with k-mers unique to the assembly presumed to be errors. Sequence shorter than 100kbp were filtered out before QV calculation.

All phasing methods produce high-quality assemblies with QV values >53 for all haplotypes (Figure 5). hifiasm QV values ranged from 54.0 to 57.1 and Verkko QV values ranged from 53.2 to 60.0. For the Verkko assemblies, the Strand-seq and Hi-C haplotypes have similar QV scores, and both phasing methods outperform the trio haplotypes, which have a QV score on average 2.25 points lower. For the hifiasm assemblies, no haplotype strongly outperforms any other. Each Verkko HaPU has a higher QV score than the corresponding hifiasm haplotype, on average 0.6 points higher for HG00733 and 4.7 points higher for NA24385.

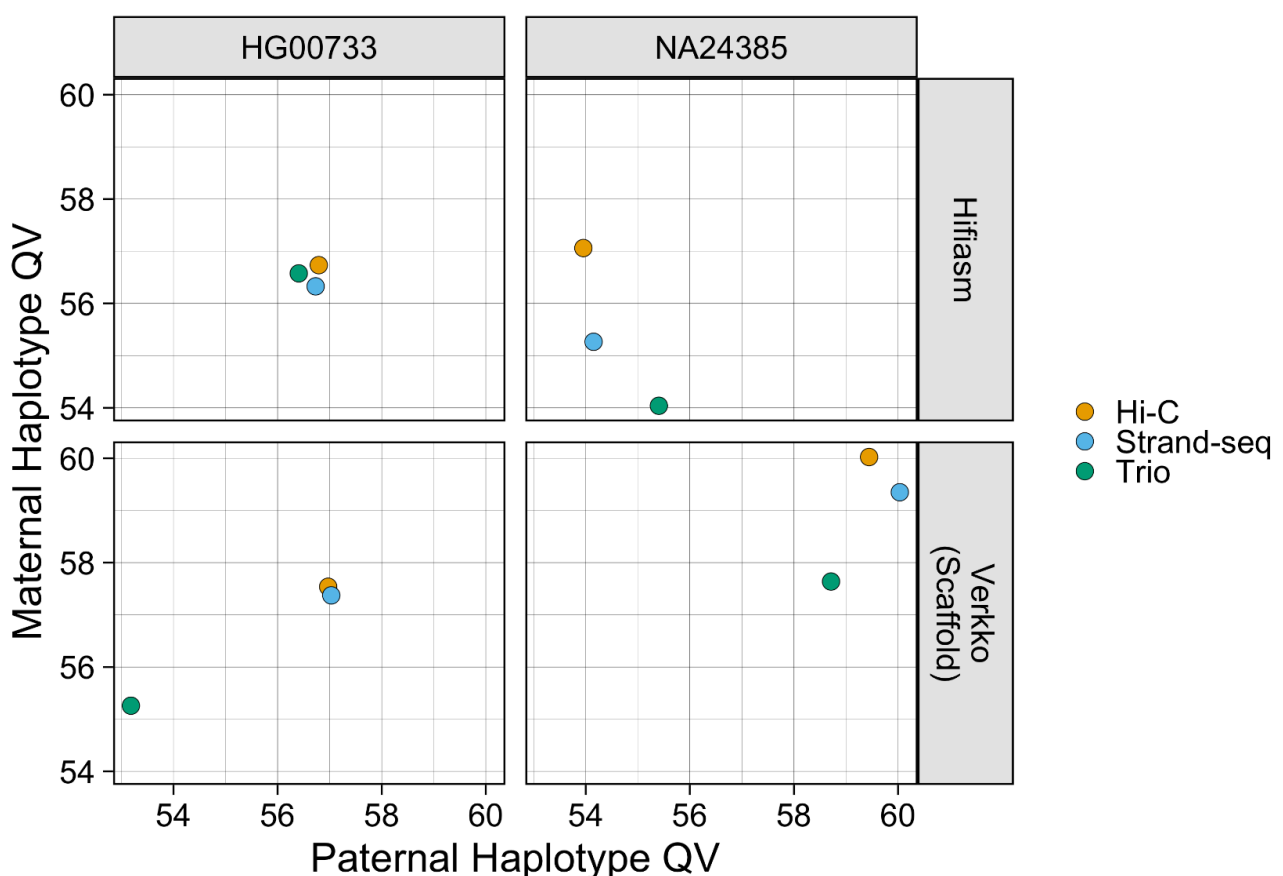


Figure 5. Assembly QV. The X-coordinate of each point is the estimated QV value of the paternal haplotype, and the Y-coordinate is the estimated QV value of the maternal haplotype. Points are colored by phasing method.

## Structural Misassemblies

Further evaluation was performed using `paftools.js`, a script included in the `Minimap2` package [50]. `'paftools misjoin'` counts gaps, inversions, and interchromosomal misjoins after aligning assembly contigs to a reference genome. The reference assemblies used were the T2T v2.0 CHM13 assembly [49] for HG00733, and the Q100 v1.0 assembly for NA24385, and alignment was performed with `minimap2`. `'paftools.js misjoin'` was run with maximum gap size and minimum alignment block length thresholds of 1 Mbp. In our evaluation, we also examined the number of issues occurring entirely on unitigs aligning to acrocentric chromosomes, which are the most difficult to properly assemble and the most difficult to evaluate with alignment-based techniques.

Across all assemblies, the number of issues reported was low, with each haplotype having no more than 9 detected events of a given category (Figure 6). Gaps were the most commonly reported event across all haplotypes, and mostly occurred on non-acrocentric chromosomes. Only the Verkko NA24385 haplotypes had no gaps detected on unitigs aligning to autosomal chromosomes. Interchromosomal misjoins were the second most common event, and were reported only in unitigs aligning to acrocentric chromosomes. Due to the large amount of repetitive sequence within and between the acrocentric chromosomes, the interchromosomal misjoins may reflect a spurious call due

to misalignment of the contigs to the reference [55]. Of the NA24385 Verkko assemblies, the trio haplotypes had the fewest events, with the maternal haplotype reporting no events, and the paternal haplotype reporting one gap and one interchromosomal misjoin, both on acrocentric chromosomes. For HG00733, performance was comparable across phasing methods, with no one haplotype obviously over or under performing the other haplotypes. Additionally, more gaps and inversions were reported for the HG00733 assemblies than for the NA24385 assemblies, which may reflect genuine variation between the sample and CHM13 reference.

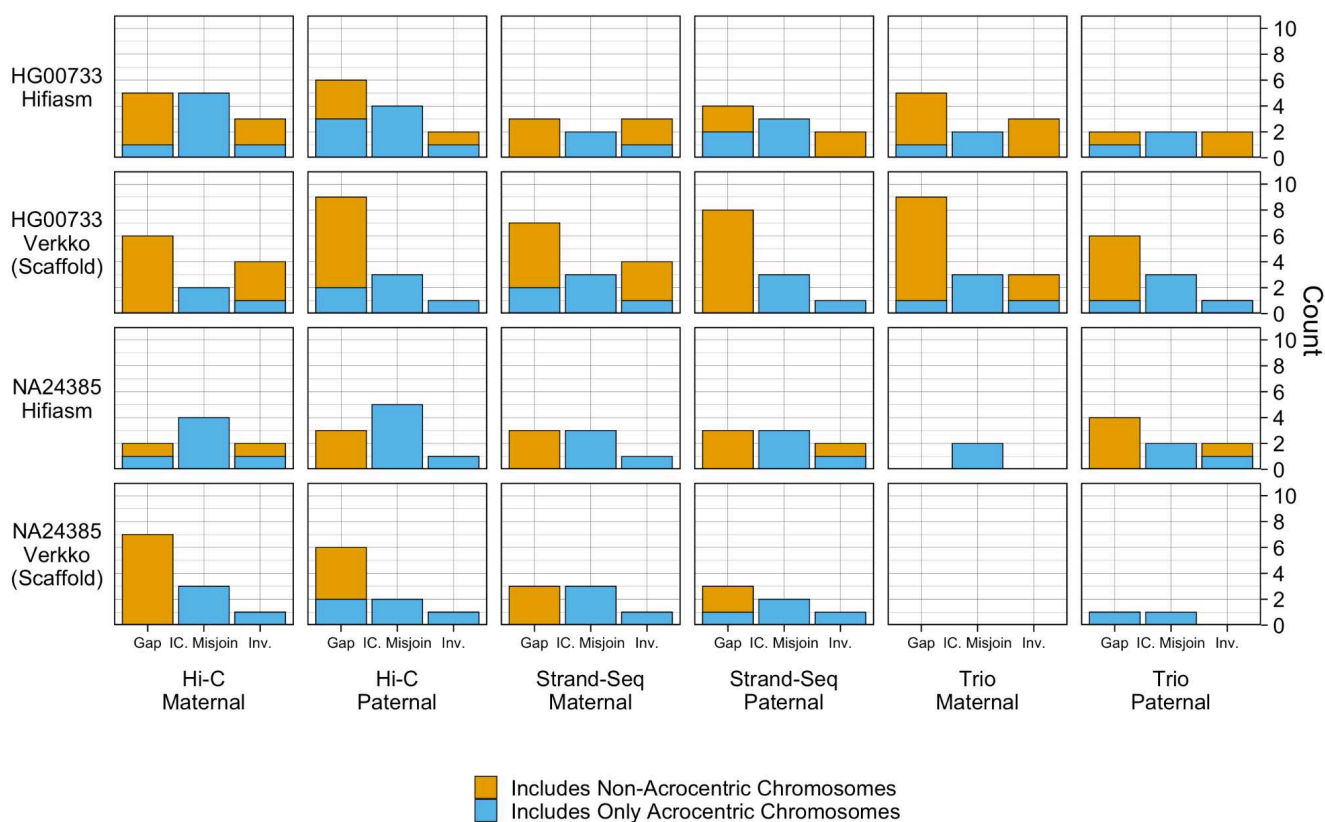


Figure 6. *paftools.js misjoin Statistics*: Three event categories are plotted: gaps, interchromosomal misjoins, and inversions. Each bar is colored blue according to the fraction of the misjoin type occurring entirely on acrocentric chromosomes (chromosomes 13, 14, 15, 21, 22).

## Gene Completeness

'paftools asmgene' detects missing genes by aligning transcripts to both an assembly haplotype and a haploid reference and counting discrepancies in gene copy number. Subsequently, the percentage of genes that are multi-copy in the haploid reference but not in the assembly haplotype (%MMC) and the percentage of genes that are single-copy in the haploid reference but not in the assembly haplotype (%MSC) was computed. The reference assemblies used were the T2T v2.0 CHM13 assembly for HG00733, and the Q100 v1.0 assembly for NA24385, the transcripts came from Gencode v.44 protein-coding sequences [56], and alignment was performed with minimap2. Each assembly haplotype was compared against the reference haplotype corresponding to the majority hap-mers

occurring on the haplotype. Only full-length alignments with at least 99% identity were considered to label a gene as 'present' for the calculation of missing multi- and single-copy genes.

The assemblies showed generally consistent patterns of gene missingness within samples (Figure 7). The NA24385 haplotypes all have an MMC under 10% and MSC under 1.0%. The MSC for the HG00733 haplotypes ranged from 0.7% to 1.2% and the MMC ranged 7.6% to 14.4% except for the Verkko trio haplotypes, where the paternal haplotype had an unexpectedly high MMC of 27.4%, and both paternal and maternal haplotypes had an unexpectedly high MSC of 4.9% and 6.0% respectively, and further investigation revealed both X chromosomes had been assigned to the maternal haplotype. Inspection of the hap-mer counts showed that the phasing signal for the X chromosome was particularly noisy, such that a haplotype could not be confidently called for one of the haplotypes. Of the NA24385 assemblies, the hifiasm trio and the Verkko Strand-seq assemblies reported no events for the X and Y chromosomes, while the other assemblies reported between 2 and 12 missing or fragmented genes. The NA24385 trio-phased assemblies had an MMC below 1.1%, outperforming the NA24385 Strand-seq and Hi-C phased. However, the evaluation of the NA24385 Strand-seq and Hi-C assemblies is deflated relative to trio, as these phasing methods produce HaPUs but are evaluated against true haplotype references. This result also suggests that the gene completeness of the HG00733 assemblies, which were not evaluated against a reference of the same sample, is greater than the results presented.

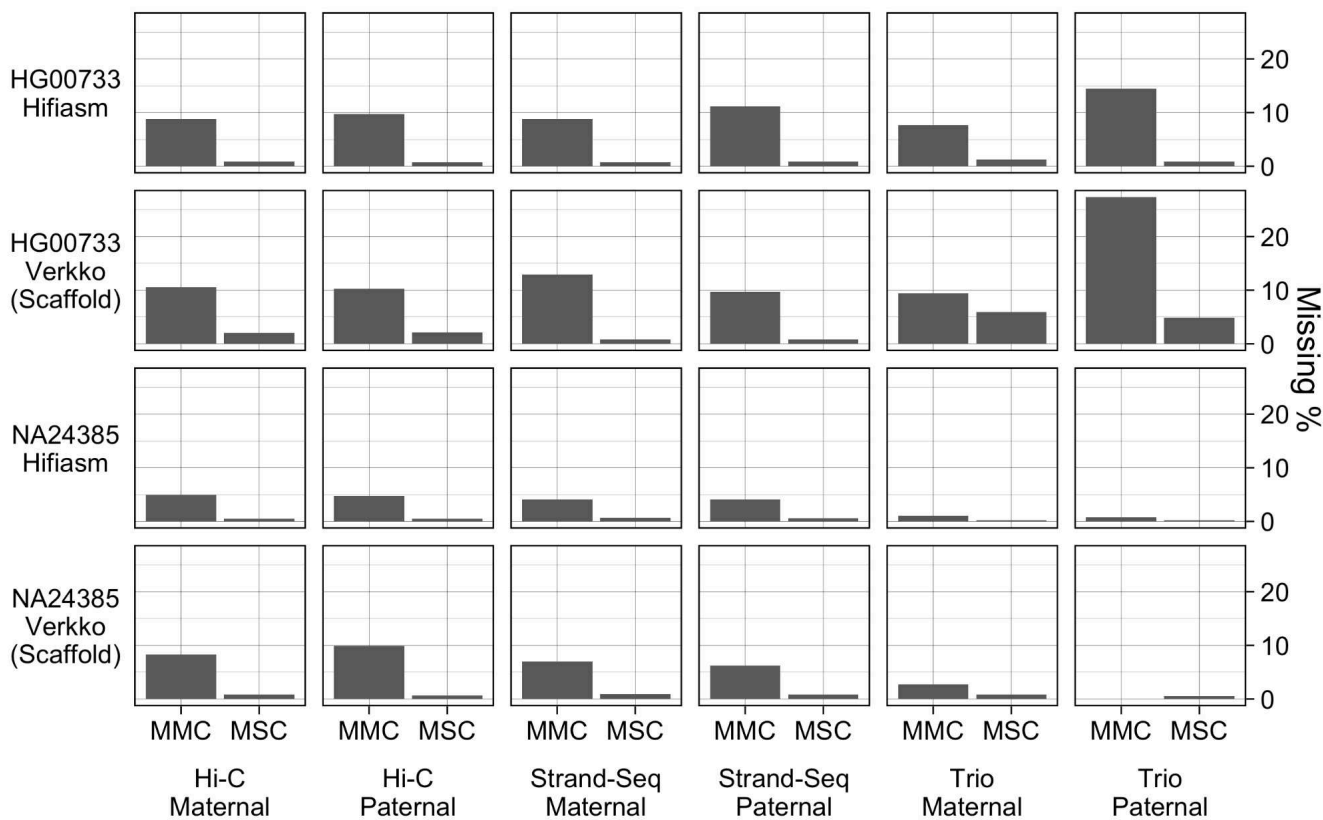
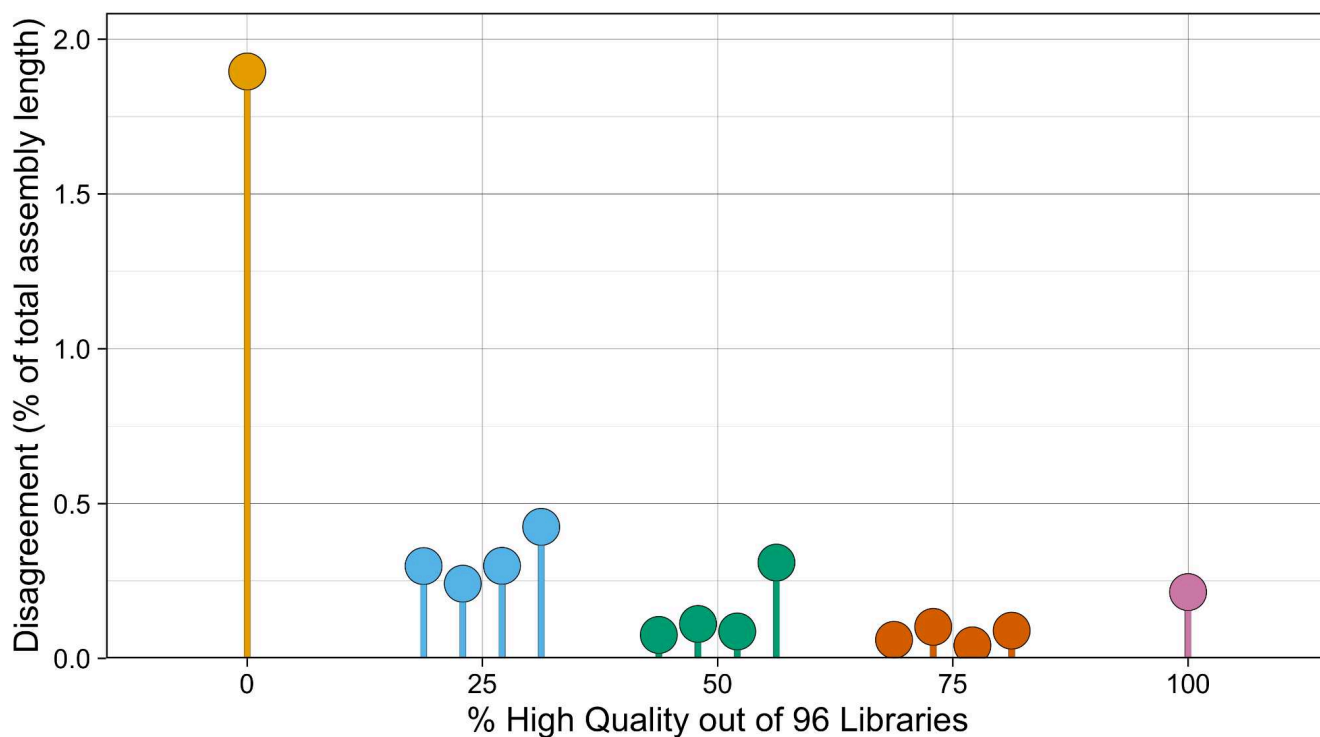


Figure 7. The fraction of missing multi-copy genes (MMC) and missing single-copy genes (MSC) calculated from `paftools.js` `asmgene` statistics.

## Strand-seq Library Titration

To evaluate the performance of Graphasing across varying Strand-seq input quality, a library titration experiment was run with the Verkko NA24385 sample. The 192 Strand-seq libraries had been previously annotated for quality, with 96 libraries labeled “high-quality” and libraries with a higher noise level and less clear phasing signal labeled “not-high-quality” (Table S1). With these annotations, 96 library sets were constructed by sampling without replacement 0%, 25%, 50%, 75%, or 100% of the libraries from the “high-quality” set, and sampling without replacement the remainder from the “not-high-quality” libraries. We sampled sets of size 96, as 96 is the number of libraries that is typically prepared in a single Strand-seq data preparation run. For the 0% and 100% library sets, as there is only one way to sample 0% or 100% of a set, there is only one sampled set. For each of the other percentages, four library sets were generated. Each sampled library set was then input to Graphasing, and the output haplotype coloring was compared against the haplotype coloring made with all 192 libraries as a reference. Disagreement with the reference was quantified as the percentage of the total assembly size, calculated using unitigs larger than the 250kbp input threshold, whose coloring does not match the reference.

Our titration experiment showed that results generally improved with the fraction of high-quality libraries, with libraries above 75% high-quality showing greater than 99.75% agreement with the reference (Figure 8). Within each high-quality fraction, variance was small, and all library sets with at least 25% high-quality libraries showed disagreement below 0.5%. The performance gains beyond 50% high-quality libraries were small but consistent, with all 75% high-quality library sets showing disagreement below 0.1%. Curiously, the library set with 100% high-quality libraries showed higher disagreement with the reference than any 75% library set, the result of disagreement on a single 5Mbp unitig (Figure S4). We additionally inspected the auN of the resulting scaffolds for each titrated set, and found that all samples achieved an auN within 8% of the reference auN, indicating that contiguity was also maintained across varying library compositions (Table S2). Our results indicate that high-quality phasing can be achieved across the entire range of Strand-seq input quality, as even a set of 96 low-quality libraries can still produce contiguous assembly with greater than 98% concordance with a reference set of 192 Strand-seq libraries for input unitigs longer than 250kbp.



*Figure 8. Disagreement between titrated and reference haplotypes for NA24385. For each titrated Strand-seq library set, the haplotypes called by Rukki were compared to the reference haplotype calls generated using all 192 available Strand-seq libraries. Each color corresponds to a different fraction of high quality libraries sampled for the titrated library set. Disagreement is quantified as the percent of the total length of the assembly for which haplotype calls disagree with the reference calls.*

## Runtime and memory usage evaluation

We evaluated the runtime and memory usage of Graphasing for all samples and assembly workflows (Table 2). Run time and peak memory usage of the tools were measured using the Snakemake “benchmark” decorator within Graphasing. Runtime and peak job memory usage were profiled on a computing cluster, with a standard cluster user profile. On a cluster, hifiasm runtime was around 7.5 and 10.5 hours and Verkko runtime was around 3 and 5.5 hour. The majority of the difference in runtime between assemblies was due to the contiguity of the input, with more fragmented assemblies taking longer to phase. Peak single job memory usage was at most 24GB for Verkko and at most 62GB for hifiasm across all runs. The greater peak job memory usage of the hifiasm assemblies came from creating k-mer databases with Yak. Regardless, the time and resources required are a small fraction of those used during a typical genome assembly workflow.

Sample	Assembler	Execution Environment	Runtime (H:M)	Max Job Mem (GB)
HG00733	Verkko Hybrid	Cluster	2:45	20

NA24385	Verkko Hybrid	Cluster	5:22	24
HG00733	hifiasm Hybrid	Cluster	7:33	62
NA24385	hifiasm Hybrid	Cluster	10:37	62

*Table 3. Profiling Statistics*

## Discussion

We introduced Graphasing, a workflow to phase genome assembly graphs, and compared its performance to the native Hi-C and trio phasing of Verkko and hifiasm for hybrid HiFi + ONT assemblies. Graphasing achieved performance comparable to that of trio phasing, as demonstrated through evaluation of contiguity, phasing accuracy, and assembly quality. In addition, we performed titration experiments to identify the range of input data quality under which Graphasing performs well. Input 96 library sets containing at least 25% high-quality Strand-seq libraries consistently produced results nearly identical to those produced using 192 Strand-seq libraries, and even library sets containing only high-noise libraries still achieved greater than 98% concordance with the 192 library set. Graphasing is modular and comprehensive, wrapping all operations from alignment to scaffolding, and adaptable to any assembler that outputs an assembly graph and has a phased assembly mode, making Graphasing widely applicable to different workflows.

In our evaluations, Verkko produced assemblies with similar contig-level contiguity as hifiasm for all HG00733 assemblies and for the NA24385 Strand-seq and Hi-C assemblies. This result, when coupled with the fact that the Verkko scaffolds had similar or greater performance in assembly quality and phasing accuracy when compared to hifiasm contigs, represents an advantage for the Verkko assembler. Of the Verkko assemblies, all three phasing methods produced haplotypes with similar scaffold Nx curves and structural assembly quality and reconstructed the NA24385 X and Y chromosomes in one scaffold. However, the trio assemblies had lower QV scores and a misassigned chromosome, and the Hi-C assemblies had higher phasing error. Accordingly, we can state that the Verkko + Graphasing produced the highest-quality haplotypes.

The high contiguity of hybrid assemblies can present a unique methodological hurdle, despite the apparent decrease in phasing difficulty that comes from greater contiguity. Highly contiguous assemblies can contradict heuristics and challenge methods developed for more fragmented input. Another challenge of contiguous assemblies is when degenerate sequence is assembled alongside non-degenerate sequence onto a unitig; Degenerate genome regions receive alignments from multiple chromosomes, creating noise which can overwhelm phasing signal. The cosine-similarity based strategies utilized by Graphasing are robust to this noise and allow these challenging unitigs to be properly phased without preprocessing (Figure S5). Furthermore, Graphasing incorporates graph topology into the phasing process, allowing for a more robust phasing process that takes advantage of

the highly contiguous graphs of hybrid assemblies. Analysis of the phased haplotypes is also a challenge, as "ceiling effects" in quality analysis may pose an obstacle to accurately evaluating high-quality haplotypes.

Further downstream refinement and analyses of the phased assemblies, such as scaffolding acrocentric short arms or detection and analysis of inversions, can also be conducted with Strand-seq [57,58]. These analyses are facilitated by Strand-seq annotations computed by Graphasing. For example, one annotation identifies the phase-informative Strand-seq libraries, which allows for more informed investigation of apparent misjoins found in the assembly by allowing switch errors and misorientation events to be immediately distinguished from one another.

Graphasing is currently limited to diploid genomes. Extension to higher ploidy would require more input Strand-seq data as well as a significant rework of the core of the phasing workflow. Graphasing's cosine-similarity approaches are effective for contiguous assemblies, but can struggle with more fragmented assemblies, as the approaches that work efficiently and effectively for contiguous assemblies can lead to trouble if there are many fragmented and degenerate unitigs in the input assembly. Strand-seq data can also be difficult to produce, given the need to isolate a single cell after a cycle of cell division. However, production of Strand-seq data is improving [59]. Currently, Graphasing does not attempt to detect switch errors in the input assembly, and any switch errors present in the input assembly will propagate to the final haplotypes. Future iterations of the pipeline could include switch error detection and correction, a task for which Strand-seq already has proven successful [60].

## Conclusion

Graphasing is a Strand-seq-based phasing workflow that reconstructs chromosome-scale haplotypes from assembly graphs of diploid genomes. Comparison to gold-standard trio phasing shows that Graphasing achieves comparable performance across a range of evaluations of completeness, contiguity, and quality, and furthermore produces more complete and accurately phased assemblies than Hi-C phasing. Graphasing's modular design allows it to be easily adapted to different assembly workflows. Both the phased genomes, as well as output Strand-seq annotations, facilitate further downstream analyses, such as missassembly detection, analysis of structural variants, and haplotype-specific gene analysis.

## Methods

### Aligning reads to assembly

While all reads can be used to cluster unitigs by chromosome, only a subset of reads convey haplotype information and are useful for phasing. Accordingly, reads are aligned to the assembly twice: once with bwa mem in paired-end mode [61], to derive the alignments used for clustering and orientation

correction, and once with bwa fastmap [61] to identify the phasing-informative reads. bwa fastmap identifies super maximal exact matches (SMEMs), maximal exact matches that are not contained in any other maximal exact matches. Filtering to reads with only one SMEM filters out alignments to sequence that is present in multiple copies in the graph. This retains alignments to homozygous nodes and alignments that overlap heterozygous variation on diploid nodes. As bwa fastmap does not have a paired-end mode, reads are first merged with PEAR [62] to maximize utilized information. In cases where reads are not successfully merged, the first mate read is retained. Reads are homopolymer compressed before alignment for Verkko assemblies, as the Verkko assembly graph is also homopolymer compressed.

## Alignment Counting

Both the unitig clustering and phasing steps use only the aggregated counts of alignments in Watson and Crick orientation from each Strand-seq library. The processing steps before counting differs for each aligner. For the bwa mem alignments, duplicates are marked using sambamba [63] and then filtered out, along with supplementary, secondary, and improper alignments. bwa fastmap alignments are simply filtered to reads with only one SMEM. After filtering, the number of first-mate read alignments in Watson and Crick orientation from each Strand-seq library are counted for each unitig in the graph.

## Connected Components

The clustering step utilizes connected component information from the graph, following the heuristic that unitigs in the same connected component are more likely to have originated from the same chromosome than those in different connected components. However, unitigs from the five acrocentric chromosomes are expected to always be tangled together due to the high sequence similarity in the rDNA array. In an attempt to increase the utility of the connected component heuristic, Graphasing attempts to separate the acrocentric chromosomes before calculating the connected components. To do this, the largest connected component by number of base-pairs is first identified as the putative acrocentric cluster component. Subsequently, all nodes shorter than a threshold length, set by default to 250 kbp, are identified, and the largest tangle consisting solely of these short nodes on the putative acrocentric cluster component is labeled as the rDNA tangle. Nodes from the tangle, along with all edges connected to them, are then removed from the graph prior to calculation of connected components.

## Length Filtering

Unitigs shorter than an input threshold, which we set to 250kbp, are filtered out. The goal is to prevent short unitigs, which may either receive too few alignments to have a reliable signal or consist entirely of degenerate sequence, from adding noise that may disrupt accurate phasing of the assembly.

## Unitig Clustering

This step combines unitigs from homologous chromosomes into the same cluster. Unitig clustering can be broken into two stages: the first stage uses pre-processing and clustering functions from the contiBAIT R package [39] to form an initial clustering using only unitigs with strong clustering signal. Second, this clustering is refined and completed using a cosine-similarity based clustering strategy and additional heuristics.

Strand-seq based chromosome clustering strategies [22,37,39,40] all rely on identifying shared patterns in the unitig strand state inherited across libraries. Each pair of homologous chromosomes inherits either a heterozygous WC/CW strand state, or a homozygous WW/CC strand state for each Strand-seq library. Accordingly, all unitigs derived from the same pair of homologous chromosomes are expected to share strand states across Strand-seq libraries, making the unitig strand state a viable clustering signal. Though the exact strand state cannot be determined for each unitig and library, evidence for a homozygous or heterozygous strand state can be quantified using the *strand state frequency* (SSF); let  $w$  and  $c$  be the number of Watson and Crick reads aligning to a unitig respectively. The SSF is defined as:  $(w - c)/(w + c)$ . For a unitig with an equal number of Watson and Crick alignments, the SSF will be equal to 0, and when the alignments are all Watson or all Crick, the SSF will be 1 or -1 respectively. We therefore expect a homozygous strand state to produce SSF with a magnitude close to 1, and a heterozygous strand state to result in an SSF close to 0. The SSF for a set of Strand-seq libraries is represented as a vector, where each component of the vector corresponds to a different Strand-seq library, and the value corresponds to the SSF for the library.

### contiBAIT preprocessing and clustering

The contiBAIT preprocessing and clustering functions use a simple threshold to discretize the SSF and call strand states for each Strand-seq library. The preprocessing function then evaluates the unitigs and libraries for quality based on expected patterns in the strand states; because each unitig is expected to inherit heterozygous and homozygous strand states in a 50/50 ratio across Strand-seq libraries, large deviations from this ratio indicate possible issues. Consequently, unitigs that inherit too many heterozygous strand states across libraries, indicating possible chimerism or degenerate sequence, and libraries with too many heterozygous strand states across unitigs, indicating possible failure of the Strand-seq chemistry, are discarded. Furthermore, unitigs and libraries with too few alignments to confidently call strand state are discarded. Unitigs with too many homozygous strand states are not discarded, as this pattern of strand state inheritance is expected for haploid chromosomes, as occurs with human male genomes, where the X and Y chromosomes each have no homolog.

After preprocessing, a discrete clustering algorithm [64] is used to create an initial clustering of unitigs. To account for possible misorientations, contiBAIT uses the absolute value of the SSF for clustering. The preprocessing parameters are set such that only “well-behaved” unitigs, those for which a strand

state can be confidently called in more than 20 libraries, are used to create the clusters. This creates an initial clustering unlikely to be affected by noise which anchors the later cosine-similarity clustering.

#### contiBAIT haploid cluster identification

In each cluster, the fraction of homozygous strand states for each unitig across all libraries is calculated. If the fraction is below a threshold, set to 0.333, then the cluster is labeled as a putative haploid X/Y chromosome cluster. This only affects the downstream step which handles the pseudoautosomal regions ([PAR](#)).

#### Small cluster removal

Downstream cluster refinement is sensitive to erroneous clusters in the initial clustering. Often, erroneous clusters consist of only a few unitigs which contain a high fraction of degenerate sequence and are spread across multiple connected components. Accordingly, clusters are filtered according to coverage of connected components; For each connected component, the fraction of the component base pairs assigned to each cluster is calculated, and the unitigs from clusters covering less than 15% of the component are flagged. Subsequently, each flagged unitig is unassigned from its cluster.

#### Stochasticity warning

The clustering algorithm used by contiBAIT is a stochastic algorithm whose results may vary even when rerun with identical input. The clustering settings are set to attempt to deliberately reduce the effect of the stochasticity. Nevertheless, we have occasionally observed large errors in clustering which propagated to produce large phasing errors. These events have occurred even after many tens of clustering runs on the same input produced the same output.

### Absolute Cosine Similarity Clustering

To understand why *absolute cosine similarity* is an appropriate metric for clustering unitigs by chromosome, we first consider the behavior of the SSF for ideal Strand-seq alignment data. Under ideal conditions, each unitig would have an SSF value of 0 for each library that inherited a heterozygous strand state, and a value of 1 or -1 for each library that inherited a homozygous strand state. When considering the vector representation of the SSF, we see that *unitigs from the same chromosome will have strand state frequency vectors that point in the same direction (Figure S5)*. The cosine similarity between two vectors  $a$  and  $b$  is defined as  $||a|| ||b|| \cos\theta$  where  $\theta$  is the angle between  $a$  and  $b$ , and simplifies to  $\cos\theta$  if vectors  $a$  and  $b$  are unit-normalized. We thus see that the unit-normalized cosine similarity between two absolute SSF vectors is maximized when they point in the same direction, making it an apt similarity metric for clustering. However, there is still a risk of misclustering misorientied unitigs, which can appear to originate from a different chromosome due to having a flipped signal in homozygous strand state libraries. To account for possible misorientations, the absolute value of the cosine similarity is used for clustering.

Furthermore, Cosine similarity is an appropriate metric for use with highly contiguous assemblies, where degenerate sequence becomes more likely to be assembled onto unitigs containing non-degenerate sequence. Repetitive genome regions receive alignments from multiple chromosomes, generating phasing noise. The cosine similarity based strategies utilized by Graphasing are robust to the noise generated by degenerate regions and allow challenging unitigs to be properly phased without preprocessing. This results from the noteworthy property of cosine similarity that it reflects a relative, rather than absolute, comparison of the individual vector dimensions. Degenerate genome regions attract alignments from multiple chromosomes, and thus appear to have a homozygous strand state in every Strand-seq library. A degenerate region therefore shrinks each dimension of the SSF. However, because each non-zero component of the absolute SSF vector has a uniform magnitude, its normalized cosine similarity will not change if each dimension is shrunk by the same amount, making the metric robust to the effects of degenerate regions. An implicit assumption made by this metric is that inheriting a WC strand state in every library is impossible. While such an inheritance pattern is not ruled out by theory, it is extremely unlikely under the expectation that at least 96 Strand-seq libraries are input to the pipeline, 96 being the number of libraries generated in a single Strand-seq sequencing run. Therefore, we consider it safe to assume that an all WC inheritance pattern is almost certainly the consequence of degenerate genomic regions.

### Absolute Cosine Similarity Cluster Merging

The initial contiBAIT clustering is refined by merging highly similar clusters. We define cluster similarity as the mean of the pairwise absolute cosine similarity calculated between the unitigs in each cluster. After calculating the cluster similarities, the largest similarity value is compared to a threshold value, and if the similarity exceeds the threshold, the clusters are merged. This is repeated until no clusters are more similar than the specified threshold. When a haploid cluster is one of the clusters being merged, then the merged cluster will also be labeled as a haploid cluster. Cluster merging is first performed on each connected component with a threshold value of 0.5, before a general merging step is performed with a threshold value of 0.66. This follows the heuristic, introduced above, that unitigs on the same connected component have a higher chance of originating from the same chromosome.

### Absolute Cosine Similarity Agglomerative Clustering

The current clusters now anchor the cosine similarity clustering that will attempt to cluster the remaining unitigs. An important note is that unitigs that the cosine-similarity clustering attempts to cluster all unitigs, even those that were discarded during contiBAIT QC. The first part is a loop that only adds unitigs to existing clusters, and begins by calculating the similarity between each unclustered unitig and each cluster. We define the similarity between an unclustered unitig and a cluster the same as the similarity between two clusters: the mean of the pairwise absolute cosine similarities. The maximum similarity value is then compared to the threshold value 0.5, and if greater, the corresponding unitig is added to the corresponding cluster, and the loop repeats. When no similarities are greater than the threshold, then the algorithm shifts to a cluster creation step, where first, pairwise absolute cosine similarities are computed between the unassigned unitigs. The maximum similarity value is then compared to the threshold value 0.5, and if greater, a new cluster, containing the

two corresponding unitigs, is created. The algorithm then starts a new cluster addition loop. The clustering process ends when there are no similarities greater than the respective thresholds for the cluster addition and cluster creation steps.

### Cluster Propagation and Merging

The number of clusters on each connected component is counted and, if there is only 1 cluster, the unclustered unitigs on the connected component are assigned to the cluster. Then, another round of cosine similarity cluster merging is conducted, as described in the earlier “[Absolute Cosine Similarity Cluster Merging](#)” step.

### Pseudo-Autosomal Region (PAR) Detection

If any clusters have been labeled haploid, then the connected components on which the haploid clusters reside are inspected. If the haploid cluster covers more than 90% of the connected component, and if there also exists a diploid cluster under 2.8 Mbp in size on that connected component, then the small diploid cluster is presumed to correspond to be the PAR found on the X and Y chromosomes. Accordingly the small diploid cluster is merged into the haploid cluster. This step is necessary to ensure that the PAR and sex chromosomes are correctly phased together; because Strand-seq produces a pseudo-haplotype assembly, the PAR must be clustered with the haploid cluster before phasing to avoid a potential switch error.

### Small Cluster Removal

The cosine similarity clustering process will occasionally create erroneous clusters containing a small number of degenerate nodes from multiple chromosomes. As large, chromosome-sized clusters are expected at this stage of clustering, clusters containing less than 10Mbp are flagged as spurious and the unitigs in those clusters are unassigned.

## Cosine Similarity Unitig Orientation Correction

Before haplotype markers can be assigned, misoriented unitigs need to be detected and corrected. In contrast to the chromosome clustering step, orientation correction uses the non-absolute cosine similarity for clustering. The SSF vectors of unitigs in opposite orientation from the same chromosome will point in opposite directions, and therefore possess minimal cosine similarity. Accordingly, there is a natural clustering of the SSF vectors, with each cluster containing unitigs in the same orientation. To capture this structure, a two-cluster hierarchical clustering is calculated on the pairwise *cosine distance*, defined as  $1 - \text{cosine similarity}$ . After clustering, the unitigs from an arbitrarily chosen cluster are corrected by “flipping” their orientation so that all unitigs in the cluster now have the same orientation. However, for graphs constructed with extremely high coverage data, the hierarchical clustering may capture structure other than unitig orientation. This risk arises from the fact that the unitigs from high-coverage hybrid assemblies can be extremely long and contiguous, such that a chromosome cluster may consist of only a few unitigs. In these cases, it is not unlikely that all unitigs may already be in the same orientation, meaning the bisected structure is not present for the

hierarchical clustering to capture. To eliminate this risk, the clustering is performed on the unitigs together with a copy with the orientation “flipped”, which guarantees that unitigs in both orientations will be present when clustering. Afterwards, only the original version of each unitig is retained.

## Haplotype Informative Strand-seq library pooling

The sparse coverage of a typical Strand-seq library, generally ranging between 0.01x and 0.2x of the haploid genome [65], means that phase information from many libraries must be pooled to achieve a high quality result. Pooling haplotype informative reads requires two steps; identifying the heterozygous strand state libraries, which are the libraries that convey phasing information, and properly assigning Watson and Crick labels to reads, such that all Watson reads are assigned to one haplotype and all Crick reads to the other haplotype (Figure S6). Previous work leverages identified SNVs [41] or homologous unitig pairs [66] to provide a supervising signal in a minimum error correction framework to achieve this goal. Graphasing pools Strand-seq libraries using a self-supervised strategy requiring only the Strand-seq alignment data, making it computationally efficient and amenable for use with high coverage assembly graphs, where identification of homologous unitigs can be difficult. Once again, the SSF vector is utilized, but now calculated using only the haplotype informative alignments.

### One-Haplotype Cluster Detection and Haplotype Marker Assignment

An occasionally observed outcome of the clustering is that, for particularly high coverage assembly graphs, the two haplotypes of a chromosome will cluster separately. In our experience, this is most frequently observed with the haploid X and Y chromosomes. Because subsequent steps assume the presence of two haplotypes within each cluster, these one-haplotype clusters need to be identified and their Strand-seq libraries pooled with an alternate strategy.

To detect clusters with only one haplotype, agglomerative clustering is performed using the cosine similarity. If only one cluster is returned, it is presumed that only one haplotype is present. To avoid detection of spurious clusters, short unitigs and noisy unitigs are not used for the agglomerative clustering. The agglomerative clustering is performed by successively merging the most similar clusters until no clusters are more distant than the threshold value of 0.5.

To pool libraries, each cluster is first arbitrarily labeled a Watson or Crick cluster. Next, the Watson and Crick labels for the reads in each library are assigned such that, for each library, the count of alignments in the assigned orientation is greater than the alternative orientation. Finally, the libraries are pooled by summing up the alignments in each orientation across libraries.

### Two Haplotype Cluster Haplotype Marker Assignment

When the SSF is calculated using haplotype informative reads, unitigs from different haplotypes point in opposite directions along axes corresponding to heterozygous strand state libraries, with homozygous unitigs lying on the line between them. These three vectors lie in a plane spanned by

basis vectors which identify the strand state pattern across libraries; the heterozygous basis vector has a value of 0 for each dimension corresponding to a homozygous library, and a uniform non-zero magnitude for the heterozygous libraries, and vice versa for the homozygous basis vector. As stated previously, pooling Strand-seq libraries requires two steps; identifying the heterozygous strand state libraries, and finding the correct labeling of reads. It is sufficient to identify the basis vector corresponding to the heterozygous strand state libraries to complete both of these steps. The algorithm to identify the heterozygous basis vector leverages a self-supervised strategy utilizing the original and “flipped” versions of each unitig. First, the plane in which the data lies is captured by projecting the data onto the first two principal components. Next, a logistic regression classifier is trained to classify the original and “flipped” versions of the cluster unitigs. The key insight is that the classification boundary is parallel to the heterozygous basis vector, and consequently the heterozygous libraries can be directly identified from the non-zero components of the vector characterizing the classification boundary (Figure S7). Furthermore, the correct pooling of Watson and Crick reads can easily be identified; Given a correct pooling of reads, all non-zero components of the heterozygous basis vector should have the same sign. Therefore, a proper pooling is achieved by simply swapping label assignments for all components with a negative sign.

With real data, the heterozygous basis vector has non-zero magnitude in all components, with the larger values corresponding to putative WC libraries. Rather than thresholding the components to identify WC libraries before pooling, a weighting method is used instead. First, the heterozygous basis vector is unit-normalized. Then, the counts in each library are multiplied by the square of the corresponding component of the normalized vector. Next, the shrunken counts are scaled back such that the total counts across all libraries is the same as before shrinking. This creates “weighted pseudo-counts” where counts from WW libraries have been moved to WC libraries. Finally, the libraries are pooled by summing up the weighted pseudo-counts in each orientation across libraries for each unitig.

### Haplotype Relabeling

This step adjusts pooled counts to attempt to construct haplotypes of the same size. This step is necessary to correct large imbalances in size between haplotypes that can result from assigning multiple one-haplotype clusters to the same haplotype. Unitigs are temporarily assigned to a haplotype according to their majority read count, and the size in basepairs of each temporary haplotype is calculated. The absolute value of the log of the ratio of the haplotype sizes serves as the haplotype balance score. For each cluster, the score is computed before and after swapping the haplotype labels for that cluster. If any swap produces a lower score, then the swap producing the lowest score is executed. This algorithm loops one hundred times before completion.

## Haplotype Calling and Phased Consensus

Rather than call haplotypes for each unitig based on the pooled library counts alone, the counts are input to Rukki to be synthesized with graph topology and improve haplotype calls. The pooled counts

create an initial shading of the graph, which is subsequently refined with Rukki graph-walking heuristics before a final haplotype call is output for each unitig. Rukki additionally outputs haplotype scaffold paths in .gaf or .tsv format.

Currently, Graphasing generates files which may be input to the Verkko and hifiasm pipelines to generate a phased assembly .fasta. For Verkko, the haplotype scaffold paths can be directly input. For hifiasm, an indirect path must be taken to input the phasing information; a Yak kmer database is generated from each set of phased unitigs, which can be input to hifiasm trio mode to generate haplotype sequences.

## Declarations

### Availability of Data and Materials

Data analyzed in this study are all available from public repositories. NA24385 ONT data were acquired from the EPI2ME project and are available from the public Amazon S3 bucket s3://ont-open-data/. Data for which an ENA accession ID is listed can be accessed through the European Nucleotide Archive browser (<https://www.ebi.ac.uk/ena/browser/home>) while other data sources have a direct url (Table 3).

Sample	Data Type	ENA Accession/URL
NA24385	Strand-seq	<a href="#">url</a>
HG00733	Strand-seq	PRJEB12849
NA24385	Illumina (Phasing)	PRJNA477862
HG00733	Illumina (Phasing)	PRJNA477862
HG00733	Illumina (Evaluation)	PRJEB36890 (ERR3988823)
HG00732	Illumina (Evaluation)	PRJEB31736 (ERR3241755)
HG00731	Illumina (Evaluation)	PRJEB31736 (ERR3241754)
HG00733	HiFi (Assembly)	<a href="#">url</a> <a href="#">url</a>
NA24385	HiFi (Assembly)	PRJNA731524 PRJNA813010
HG00733	ONT (Assembly)	<a href="#">url</a> <a href="#">url</a>

NA24385	ONT (Assembly)	<a href="#">url</a>
What	Url	
Gencode Transcripts	<a href="#">url</a>	
T2T-CHM13v2.0 Assembly	<a href="#">url</a>	
NA24385 Q100 v1.0 Assembly	<a href="#">url</a>	

*Table 3. Data availability*

## Acknowledgments

The authors thank Julian Lucas (UC Santa Cruz Genomics Institute) for his assistance in identifying data sources and providing guidance on Yak use and end-to-end haplotype identification.

## Authors' Contributions

MG, DP, and TM designed an earlier version of a workflow to phase Hifi-based graphs using Strand-seq, which was implemented by MG. Based on this initial workflow, MH, PE, and TM designed the Graphasing method. MH implemented Graphasing. MH, WH and PE ran the assembly experiments. SK provided guidance on the integration with Verkko. MH prepared figures and wrote a draft manuscript. TM and PE edited the manuscript. MG and EEE helped with result interpretation and provided feedback on the manuscript. All authors read and approved the final manuscript

## Funding

This work was funded in part by the National Human Genome Research Institute of the National Institutes of Health under award numbers U24HG007497 & R01HG010169 (to E.E.E) and by the German Research Foundation under award number 496874193. E.E.E. is an investigator of the Howard Hughes Medical Institute. This work was supported, in part, by the Intramural Research Program of the National Human Genome Research Institute, National Institutes of Health (SK).

## References

1. Jarvis ED, Formenti G, Rhie A, Guerracino A, Yang C, Wood J, et al. Semi-automated assembly of high-quality diploid human reference genomes. *Nature* [Internet]. 2022;611:519–31. Available from: <http://dx.doi.org/10.1038/s41586-022-05325-5>
2. Glusman G, Cox HC, Roach JC. Whole-genome haplotyping approaches and genomic medicine. *Genome Med* [Internet]. 2014;6:73. Available from: <http://dx.doi.org/10.1186/s13073-014-0073-7>
3. Tewhey R, Bansal V, Torkamani A, Topol EJ, Schork NJ. The importance of phase information for human genomics. *Nat Rev Genet* [Internet]. 2011;12:215–23. Available from: <http://dx.doi.org/10.1038/nrg2950>
4. Leitwein M, Duranton M, Rougemont Q, Gagnaire P-A, Bernatchez L. Using Haplotype Information for Conservation Genomics. *Trends Ecol Evol* [Internet]. 2020;35:245–58. Available from: <http://dx.doi.org/10.1016/j.tree.2019.10.012>
5. Green RE, Krause J, Briggs AW, Maricic T, Stenzel U, Kircher M, et al. A draft sequence of the Neandertal genome. *Science* [Internet]. 2010;328:710–22. Available from: <http://dx.doi.org/10.1126/science.1188021>
6. Cheng Y, Berg A, Wu S, Li Y, Wu R. Computing genetic imprinting expressed by haplotypes. *Methods Mol Biol* [Internet]. 2009;573:189–212. Available from: [http://dx.doi.org/10.1007/978-1-60761-247-6\\_11](http://dx.doi.org/10.1007/978-1-60761-247-6_11)
7. Amarasinghe SL, Su S, Dong X, Zappia L, Ritchie ME, Gouil Q. Opportunities and challenges in long-read sequencing data analysis. *Genome Biol* [Internet]. 2020;21:30. Available from: <http://dx.doi.org/10.1186/s13059-020-1935-5>
8. Wenger AM, Peluso P, Rowell WJ, Chang P-C, Hall RJ, Concepcion GT, et al. Accurate circular consensus long-read sequencing improves variant detection and assembly of a human genome. *Nat Biotechnol* [Internet]. 2019;37:1155–62. Available from: <http://dx.doi.org/10.1038/s41587-019-0217-9>
9. Jain M, Koren S, Miga KH, Quick J, Rand AC, Sasani TA, et al. Nanopore sequencing and assembly of a human genome with ultra-long reads. *Nat Biotechnol* [Internet]. 2018;36:338–45. Available from: <http://dx.doi.org/10.1038/nbt.4060>
10. Cheng H, Jarvis ED, Fedrigo O, Koepfli K-P, Urban L, Gemmell NJ, et al. Haplotype-resolved assembly of diploid genomes without parental data. *Nat Biotechnol* [Internet]. 2022;40:1332–5. Available from: <http://dx.doi.org/10.1038/s41587-022-01261-x>
11. Rautiainen M, Nurk S, Walenz BP, Logsdon GA, Porubsky D, Rhie A, et al. Telomere-to-telomere assembly of diploid chromosomes with Verkko. *Nat Biotechnol* [Internet]. 2023; Available from: <http://dx.doi.org/10.1038/s41587-023-01662-6>
12. Garg S. Computational methods for chromosome-scale haplotype reconstruction. *Genome Biol* [Internet]. 2021;22:101. Available from: <http://dx.doi.org/10.1186/s13059-021-02328-9>

13. Sedlazeck FJ, Lee H, Darby CA, Schatz MC. Piercing the dark matter: bioinformatics of long-range sequencing and mapping. *Nat Rev Genet* [Internet]. 2018;19:329–46. Available from: <http://dx.doi.org/10.1038/s41576-018-0003-4>
14. Nurk S, Koren S, Rhie A, Rautiainen M, Bzikadze AV, Mikheenko A, et al. The complete sequence of a human genome. *Science* [Internet]. 2022;376:44–53. Available from: <http://dx.doi.org/10.1126/science.abj6987>
15. Patterson M, Marschall T, Pisanti N, van Iersel L, Stougie L, Klau GW, et al. WhatsHap: Weighted Haplotype Assembly for Future-Generation Sequencing Reads. *J Comput Biol* [Internet]. 2015;22:498–509. Available from: <http://dx.doi.org/10.1089/cmb.2014.0157>
16. Pirola Y, Zaccaria S, Dondi R, Klau GW, Pisanti N, Bonizzoni P. HapCol: accurate and memory-efficient haplotype assembly from long reads. *Bioinformatics* [Internet]. 2016;32:1610–7. Available from: <http://dx.doi.org/10.1093/bioinformatics/btv495>
17. Edge P, Bafna V, Bansal V. HapCUT2: robust and accurate haplotype assembly for diverse sequencing technologies. *Genome Res* [Internet]. 2017;27:801–12. Available from: <http://dx.doi.org/10.1101/gr.213462.116>
18. Ebler J, Haukness M, Pesout T, Marschall T, Paten B. Haplotype-aware diplotyping from noisy long reads. *Genome Biol* [Internet]. 2019;20:116. Available from: <http://dx.doi.org/10.1186/s13059-019-1709-0>
19. Lin J-H, Chen L-C, Yu S-C, Huang Y-T. LongPhase: an ultra-fast chromosome-scale phasing algorithm for small and large variants. *Bioinformatics* [Internet]. 2022;38:1816–22. Available from: <http://dx.doi.org/10.1093/bioinformatics/btac058>
20. Masutani B, Suzuki Y, Suzuki Y, Morishita S. JTK: targeted diploid genome assembler. *Bioinformatics* [Internet]. 2023;39. Available from: <http://dx.doi.org/10.1093/bioinformatics/btad398>
21. Luo X, Kang X, Schönhuth A. phasebook: haplotype-aware de novo assembly of diploid genomes from long reads. *Genome Biol* [Internet]. 2021;22:299. Available from: <http://dx.doi.org/10.1186/s13059-021-02512-x>
22. Porubsky D, Ebert P, Audano PA, Vollger MR, Harvey WT, Marijon P, et al. Fully phased human genome assembly without parental data using single-cell strand sequencing and long reads. *Nat Biotechnol* [Internet]. 2021;39:302–8. Available from: <http://dx.doi.org/10.1038/s41587-020-0719-5>
23. Garg S, Fungtammasan A, Carroll A, Chou M, Schmitt A, Zhou X, et al. Chromosome-scale, haplotype-resolved assembly of human genomes. *Nat Biotechnol* [Internet]. 2021;39:309–12. Available from: <http://dx.doi.org/10.1038/s41587-020-0711-0>
24. Falconer E, Hills M, Naumann U, Poon SSS, Chavez EA, Sanders AD, et al. DNA template strand sequencing of single-cells maps genomic rearrangements at high resolution. *Nat Methods* [Internet]. 2012;9:1107–12. Available from: <http://dx.doi.org/10.1038/nmeth.2206>
25. Sanders AD, Falconer E, Hills M, Spierings DCJ, Lansdorp PM. Single-cell template strand sequencing by Strand-seq enables the characterization of individual homologs. *Nat Protoc* [Internet]. 2017;12:1151–76. Available from: <http://dx.doi.org/10.1038/nprot.2017.029>

26. Lieberman-Aiden E, van Berkum NL, Williams L, Imakaev M, Ragoczy T, Telling A, et al. Comprehensive mapping of long-range interactions reveals folding principles of the human genome. *Science* [Internet]. 2009;326:289–93. Available from: <http://dx.doi.org/10.1126/science.1181369>
27. Church DM, Schneider VA, Graves T, Auger K, Cunningham F, Bouk N, et al. Modernizing reference genome assemblies. *PLoS Biol* [Internet]. 2011;9:e1001091. Available from: <http://dx.doi.org/10.1371/journal.pbio.1001091>
28. Church DM, Schneider VA, Steinberg KM, Schatz MC, Quinlan AR, Chin C-S, et al. Extending reference assembly models. *Genome Biol* [Internet]. 2015;16:13. Available from: <http://dx.doi.org/10.1186/s13059-015-0587-3>
29. Rie A, McCarthy SA, Fedrigo O, Damas J, Formenti G, Koren S, et al. Towards complete and error-free genome assemblies of all vertebrate species. *Nature* [Internet]. 2021;592:737–46. Available from: <http://dx.doi.org/10.1038/s41586-021-03451-0>
30. Kim J, Lee C, Ko BJ, Yoo DA, Won S, Phillippy AM, et al. False gene and chromosome losses in genome assemblies caused by GC content variation and repeats. *Genome Biol* [Internet]. 2022;23:204. Available from: <http://dx.doi.org/10.1186/s13059-022-02765-0>
31. Koren S, Rie A, Walenz BP, Dilthey AT, Bickhart DM, Kingan SB, et al. De novo assembly of haplotype-resolved genomes with trio binning. *Nat Biotechnol* [Internet]. 2018; Available from: <http://dx.doi.org/10.1038/nbt.4277>
32. Cheng H, Concepcion GT, Feng X, Zhang H, Li H. Haplotype-resolved de novo assembly using phased assembly graphs with hifiasm. *Nat Methods* [Internet]. 2021;18:170–5. Available from: <http://dx.doi.org/10.1038/s41592-020-01056-5>
33. Lorig-Roach R, Meredith M, Monlong J, Jain M, Olsen H, McNulty B, et al. Phased nanopore assembly with Shasta and modular graph phasing with GFase. *bioRxiv* [Internet]. 2023; Available from: <http://dx.doi.org/10.1101/2023.02.21.529152>
34. Garg S, Rautiainen M, Novak AM, Garrison E, Durbin R, Marschall T. A graph-based approach to diploid genome assembly. *Bioinformatics* [Internet]. 2018;34:i105–14. Available from: <http://dx.doi.org/10.1093/bioinformatics/bty279>
35. Ouchi S, Kajitani R, Itoh T. GreenHill: a de novo chromosome-level scaffolding and phasing tool using Hi-C. *Genome Biol* [Internet]. 2023;24:162. Available from: <http://dx.doi.org/10.1186/s13059-023-03006-8>
36. Köster J, Rahmann S. Snakemake--a scalable bioinformatics workflow engine. *Bioinformatics* [Internet]. 2012;28:2520–2. Available from: <http://dx.doi.org/10.1093/bioinformatics/bts480>
37. Ghareghani M, Porubský D, Sanders AD, Meiers S, Eichler EE, Korbel JO, et al. Strand-seq enables reliable separation of long reads by chromosome via expectation maximization. *Bioinformatics* [Internet]. 2018;34:i115–23. Available from: <http://dx.doi.org/10.1093/bioinformatics/bty290>
38. Hills M, Falconer E, O'Neill K, Sanders AD, Howe K, Guryev V, et al. Construction of Whole Genomes from Scaffolds Using Single Cell Strand-Seq Data. *Int J Mol Sci* [Internet]. 2021;22. Available from: <http://dx.doi.org/10.3390/ijms22073617>

39. O'Neill K, Hills M, Gottlieb M, Borkowski M, Karsan A, Lansdorp PM. Assembling draft genomes using contiBAIT. *Bioinformatics* [Internet]. 2017;33:2737–9. Available from: <http://dx.doi.org/10.1093/bioinformatics/btx281>
40. Hills M, O'Neill K, Falconer E, Brinkman R, Lansdorp PM. BAIT: Organizing genomes and mapping rearrangements in single cells. *Genome Med* [Internet]. 2013;5:82. Available from: <http://dx.doi.org/10.1186/gm486>
41. Porubsky D, Garg S, Sanders AD, Korbel JO, Guryev V, Lansdorp PM, et al. Dense and accurate whole-chromosome haplotyping of individual genomes. *Nat Commun* [Internet]. 2017;8:1293. Available from: <http://dx.doi.org/10.1038/s41467-017-01389-4>
42. Porubský D, Sanders AD, van Wietmarschen N, Falconer E, Hills M, Spierings DCJ, et al. Direct chromosome-length haplotyping by single-cell sequencing. *Genome Res* [Internet]. 2016;26:1565–74. Available from: <http://dx.doi.org/10.1101/gr.209841.116>
43. Lander ES, Linton LM, Birren B, Nusbaum C, Zody MC, Baldwin J, et al. Initial sequencing and analysis of the human genome. *Nature* [Internet]. 2001;409:860–921. Available from: <http://dx.doi.org/10.1038/35057062>
44. Salzberg SL, Phillippy AM, Zimin A, Puiu D, Magoc T, Koren S, et al. GAGE: A critical evaluation of genome assemblies and assembly algorithms. *Genome Res* [Internet]. 2012;22:557–67. Available from: <http://dx.doi.org/10.1101/gr.131383.111>
45. Akbari V, Hanlon VCT, O'Neill K, Lefebvre L, Schrader KA, Lansdorp PM, et al. Parent-of-origin detection and chromosome-scale haplotyping using long-read DNA methylation sequencing and Strand-seq. *Cell Genom* [Internet]. 2023;3:100233. Available from: <http://dx.doi.org/10.1016/j.xgen.2022.100233>
46. Gurevich A, Saveliev V, Vyahhi N, Tesler G. QUAST: quality assessment tool for genome assemblies. *Bioinformatics* [Internet]. 2013;29:1072–5. Available from: <http://dx.doi.org/10.1093/bioinformatics/btt086>
47. Zook JM, Hansen NF, Olson ND, Chapman L, Mullikin JC, Xiao C, et al. A robust benchmark for detection of germline large deletions and insertions. *Nat Biotechnol* [Internet]. 2020;38:1347–55. Available from: <http://dx.doi.org/10.1038/s41587-020-0538-8>
48. Wang T, Antonacci-Fulton L, Howe K, Lawson HA, Lucas JK, Phillippy AM, et al. The Human Pangenome Project: a global resource to map genomic diversity. *Nature* [Internet]. 2022;604:437–46. Available from: <http://dx.doi.org/10.1038/s41586-022-04601-8>
49. Rhie A, Nurk S, Cechova M, Hoyt SJ, Taylor DJ, Altemose N, et al. The complete sequence of a human Y chromosome. *Nature* [Internet]. 2023;621:344–54. Available from: <http://dx.doi.org/10.1038/s41586-023-06457-y>
50. Li H. Minimap2: pairwise alignment for nucleotide sequences. *Bioinformatics* [Internet]. 2018;34:3094–100. Available from: <http://dx.doi.org/10.1093/bioinformatics/bty191>
51. Li H. New strategies to improve minimap2 alignment accuracy. *Bioinformatics* [Internet]. 2021;37:4572–4. Available from: <http://dx.doi.org/10.1093/bioinformatics/btab705>

52. Li H. seqtk: Toolkit for processing sequences in FASTA/Q formats [Internet]. Github; [cited 2024 Jan 26]. Available from: <https://github.com/lh3/seqtk>
53. HG002: A complete diploid human genome [Internet]. Github; [cited 2024 Jan 11]. Available from: <https://github.com/marbl/HG002>
54. Rie A, Walenz BP, Koren S, Phillippy AM. Merqury: reference-free quality, completeness, and phasing assessment for genome assemblies. *Genome Biol* [Internet]. 2020 [cited 2024 Jan 17];21:1–27. Available from: <https://genomebiology.biomedcentral.com/articles/10.1186/s13059-020-02134-9>
55. Guerracino A, Buonaiuto S, de Lima LG, Potapova T, Rie A, Koren S, et al. Recombination between heterologous human acrocentric chromosomes. *Nature* [Internet]. 2023;617:335–43. Available from: <http://dx.doi.org/10.1038/s41586-023-05976-y>
56. Frankish A, Diekhans M, Ferreira A-M, Johnson R, Jungreis I, Loveland J, et al. GENCODE reference annotation for the human and mouse genomes. *Nucleic Acids Res* [Internet]. 2019;47:D766–73. Available from: <http://dx.doi.org/10.1093/nar/gky955>
57. Porubsky D, Höps W, Ashraf H, Hsieh P, Rodriguez-Martin B, Yilmaz F, et al. Recurrent inversion polymorphisms in humans associate with genetic instability and genomic disorders. *Cell* [Internet]. 2022;185:1986–2005.e26. Available from: <http://dx.doi.org/10.1016/j.cell.2022.04.017>
58. Sanders AD, Hills M, Porubský D, Guryev V, Falconer E, Lansdorp PM. Characterizing polymorphic inversions in human genomes by single-cell sequencing. *Genome Res* [Internet]. 2016;26:1575–87. Available from: <http://dx.doi.org/10.1101/gr.201160.115>
59. Hanlon VCT, Chan DD, Hamadeh Z, Wang Y, Mattsson C-A, Spierings DCJ, et al. Construction of Strand-seq libraries in open nanoliter arrays. *Cell Rep Methods* [Internet]. 2022;2:100150. Available from: <http://dx.doi.org/10.1016/j.crmeth.2021.100150>
60. Porubsky D, Sanders AD, Taudt A, Colomé-Tatché M, Lansdorp PM, Guryev V. breakpointR: an R/Bioconductor package to localize strand state changes in Strand-seq data. *Bioinformatics* [Internet]. 2020;36:1260–1. Available from: <http://dx.doi.org/10.1093/bioinformatics/btz681>
61. Li H. Aligning sequence reads, clone sequences and assembly contigs with BWA-MEM [Internet]. arXiv [q-bio.GN]. 2013. Available from: <http://arxiv.org/abs/1303.3997>
62. Zhang J, Kober K, Flouri T, Stamatakis A. PEAR: a fast and accurate Illumina Paired-End reAd mergeR. *Bioinformatics* [Internet]. 2014;30:614–20. Available from: <http://dx.doi.org/10.1093/bioinformatics/btt593>
63. Tarasov A, Vilella AJ, Cuppen E, Nijman IJ, Prins P. Sambamba: fast processing of NGS alignment formats. *Bioinformatics* [Internet]. 2015;31:2032–4. Available from: <http://dx.doi.org/10.1093/bioinformatics/btv098>
64. O'Neill K. Automated analysis of single cell leukemia data [Internet]. University of British Columbia; 2014 [cited 2023 Oct 3]. Available from: <https://open.library.ubc.ca/soa/cIRcle/collections/ubctheses/24/items/1.0135595>
65. Hanlon V, Porubsky D, Lansdorp P. Chromosome-length haplotypes with StrandPhaseR and

Strand-seq [Internet]. The University of British Columbia; 2022. Available from: <https://doi.library.ubc.ca/10.14288/1.0406302>

66. Ghareghani M. Single-cell strand sequencing for structural variant analysis and genome assembly [Internet]. Universität des Saarlandes; 2022. Available from:

<https://publikationen.sulb.uni-saarland.de/handle/20.500.11880/34644>

67. Wick RR, Schultz MB, Zobel J, Holt KE. Bandage: interactive visualization of de novo genome assemblies. *Bioinformatics* [Internet]. 2015;31:3350–2. Available from:

<http://dx.doi.org/10.1093/bioinformatics/btv383>

68. Chin C-S, Peluso P, Sedlazeck FJ, Nattestad M, Concepcion GT, Clum A, et al. Phased diploid genome assembly with single-molecule real-time sequencing. *Nat Methods* [Internet].

2016;13:1050–4. Available from: <http://dx.doi.org/10.1038/nmeth.4035>

69. Kronenberg ZN, Rhee A, Koren S, Concepcion GT, Peluso P, Munson KM, et al. Extended haplotype-phasing of long-read de novo genome assemblies using Hi-C. *Nat Commun* [Internet]. 2021;12:1935. Available from: <http://dx.doi.org/10.1038/s41467-020-20536-y>